arXiv:1511.06920v1 [q-bio.NC] 21 Nov 2015

Cell assembly dynamics of sparsely-connected inhibitory networks: a simple model for the collective activity of striatal projection neurons

David Angulo-Garcia*
CNR - Consiglio Nazionale delle Ricerche - Istituto dei Sistemi Complessi, via Madonna del Piano 10, I-50019 Sesto Fiorentino, Italy

Joshua D. Berke†
Department of Psychology, University of Michigan, Ann Arbor, 530 Church St., Ann Arbor, MI 48104, USA

Alessandro Torcini‡
Aix-Marseille Université, Inserm, INMED UMR 901 and Institut de Neurosciences des Systèmes UMR 1106, 13000 Marseille, France
Aix-Marseille Université, Université de Toulon, CNRS, CPT, UMR 7332, 13288 Marseille, France
CNR - Consiglio Nazionale delle Ricerche - Istituto dei Sistemi Complessi, via Madonna del Piano 10, I-50019 Sesto Fiorentino, Italy and
INFN Sez. Firenze, via Sansone, 1 - I-50019 Sesto Fiorentino, Italy

Striatal projection neurons form a sparsely-connected inhibitory network, and this arrangement may be essential for the appropriate temporal organization of behavior. Here we show that a simplified, sparse inhibitory network of Leaky-Integrate-and-Fire neurons can reproduce some key features of striatal population activity, as observed in brain slices [*Carrillo-Reid et al., J. Neurophysiology* **99** *(2008) 1435–1450*]. In particular we develop a new metric to determine the conditions under which sparse inhibitory networks form anti-correlated cell assemblies with time-varying activity of individual cells. We find that under these conditions the network displays an input-specific sequence of cell assembly switching, that effectively discriminates similar inputs. Our results support the proposal [*Ponzi and Wickens, PLoS Comp Biol* **9** *(2013) e1002954*] that GABAergic connections between striatal projection neurons allow stimulus-selective, temporally-extended sequential activation of cell assemblies. Furthermore, we help to show how altered intrastriatal GABAergic signaling may produce aberrant network-level information processing in disorders such as Parkinson's and Huntington's diseases.

Author Summary
Neuronal networks that are loosely coupled by inhibitory connections can exhibit potentially useful properties. These include the ability to produce slowly-changing activity patterns, that could be important for organizing actions and thoughts over time. The striatum is a major brain structure that is critical for appropriately timing behavior to receive rewards. Striatal projection neurons have loose inhibitory interconnections, and here we show that even a highly simplified model of this striatal network is capable of producing slowly-changing activity sequences. We examine some key parameters important for producing these dynamics, and help explain how changes in striatal connectivity may contribute to serious human disorders including Parkinson's and Huntington's diseases.

* david.angulo@fi.isc.cnr.it
† jdberke@umich.edu
‡ alessandro.torcini@cnr.it

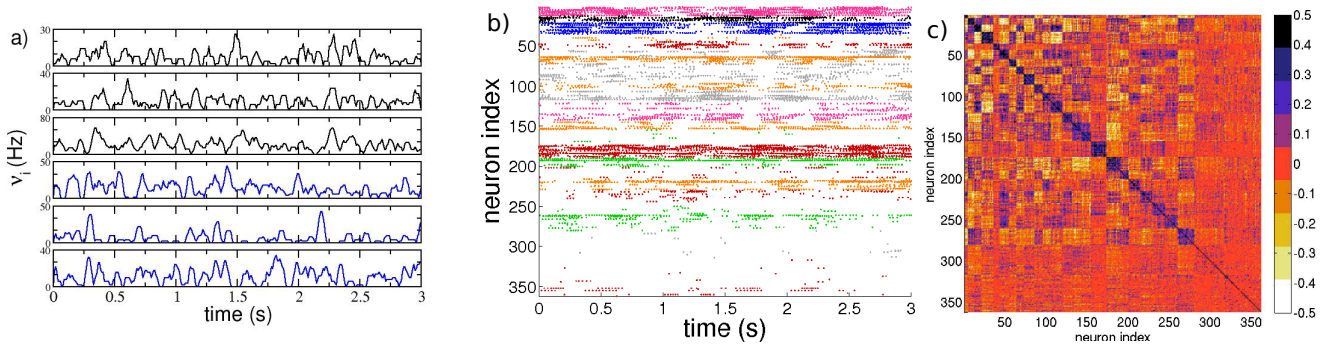

FIG. 1. **Cell activity characterization.** a) Firing rates ν_i of 6 selected neurons belonging to two anti-correlated assemblies, the color identifies the assembly and the colors correspond to the one used in b) for the different clusters; b) raster plot activity, the firing times are colored according to the assembly the neurons belong to; c) cross-correlation matrix $C(\nu_i, \nu_j)$ of the firing rates. The neurons in panel b) and c) are clustered according to the correlation of their firing rates by employing the *k-means* algorithm; the clusters are ordered in terms of their average correlation (inside each cluster) from the highest to the lowest one (for more details see Methods). The firing rates are calculated over overlapping time windows of duration 1 s, the origins of successive windows are shifted by 50 ms. The system is evolved during 10^7 spikes, after discarding an initial transient of 10^5 spike events. Other parameters used in the simulation: $g = 8$, $K = 20$, $N = 400$, $k_{mean} = N_{act}/15$, $\Delta V = 5$ mV and $\tau_\alpha = 20$ ms. The number of active neurons is 370, corresponding to $n^* \simeq 93$ %.

I. INTRODUCTION

The basal ganglia are critical brain structures for behavioral control, whose organization has been highly conserved during vertebrate evolution [1]. Altered activity of the basal ganglia underlies a wide range of human neurological and psychiatric disorders, but the specific computations normally performed by these circuits remain elusive. The largest component of the basal ganglia is the striatum, which appears to have a key role in adaptive decision-making based on reinforcement history [2], and in behavioral timing on scales from tenths of seconds to tens of seconds [3].

The great majority ($> 90\%$) of striatal neurons are GABAergic medium spiny neurons (MSNs), which project to other basal ganglia structures but also make local collateral connections within striatum [4, 5]. These local connections were proposed in early theories to achieve action selection through strong winner-take-all lateral inhibition [6, 7], but this idea fell out of favor once it became clear that MSN connections are actually sparse (nearby connection probabilities $\simeq 10 - 25\%$ [8, 9]), unidirectional and relatively weak [10, 11]. Nonetheless, striatal networks are intrinsically capable of generating sequential patterns of cell activation, even in brain slice preparations without time-varying external inputs [12, 13]. Following previous experimental evidence that collateral inhibition can help organize MSN firing [14], an important recent set of modeling studies argued that the sparse connections between MSNs, though individually weak, can collectively mediate sequential switching between cell assemblies [15, 16]. It was further hypothesized that these connections may even be optimally configured for this purpose [17]. This proposal is of high potential significance, since sequential dynamics may be central to the striatum's functional role in the organization and timing of behavioral output [18, 19].

In their work [15–17], Ponzi and Wickens used conductance-based model neurons (with persistent Na^+ and K^+ currents [20]), in proximity to a bifurcation from a stable fixed point to a tonic firing regime. We show here that networks based on simpler leaky integrate-and-fire (LIF) neurons can also exhibit sequences of cell assembly activation. This simpler model, together with a novel measure of structured bursting, allows us to more clearly identify the critical parameters needed to observe dynamics resembling that of the striatal MSN network. Among other results, we show that the duration of GABAergic post-synaptic currents is crucial for the network′s ability to discriminate different input patterns. A reduction of the post-synaptic time scale, analogous to that observed for IPSCs of MSNs in mouse models of Huntington's disease (HD) [21], leads in our model to alteration of single neuron and population dynamics typical of striatal dynamics in symptomatic HD mice [22]. Finally, we qualitatively replicate the observed response of striatal networks in brain slices to altered excitatory drive and to reduction of GABAergic transmission between axon collaterals of striatal neurons [12]. The latter effect can be induced by dopamine loss [23], therefore our results may help generate new insights into the aberrant activity patterns observed in Parkinson's disease (PD).

II. RESULTS

Measuring cell assembly dynamics

The model is composed of N leaky integrate-and-fire (LIF) inhibitory neurons [24, 25], with each neuron receiving inputs from a randomly selected 5% of the other neurons (i.e. a directed Erdös-Renyi graph with constant in-degree $K = pN$, where $p = 5\%$) [26]. The inhibitory post-synaptic potentials (PSPs) are schematized as α-functions characterized by a decay time τ_α and a peak amplitude A_{PSP}. In addition, each neuron i is subject to an excitatory input current mimicking the cortical and thalamic inputs received by the striatal network. In order to obtain firing periods of any duration the excitatory drives are tuned to drive the neurons in proximity of the supercritical bifurcation between the quiescent and the firing state, similarly to [15]. Furthermore, our model is integrated exactly between a spike emission and the successive one by rewriting the time evolution of the network as an event-driven map [27] (for more details see Methods).

Since we will compare most of our findings with the results reported in a previous series of papers by Ponzi and Wickens (PW) [15–17] it is important to stress the similarities and differences between the two models. The model employed by PW is a two dimensional conductance-based model with a potassium and a sodium channel [20], our model is simply a current based LIF model. The parameters of the PW model are chosen so that the cell is in proximity of a saddle-node on invariant circle (SNIC) bifurcation to guarantee a smooth increase of the firing period when passing from the quiescent to the supra-threshold regime, without a sudden jump in the firing rate. Similarly, in our simulations the parameters of the LIF model are chosen in proximity of the bifurcation from silent regime to tonic firing. In the PW model the PSPs are assumed to be exponentially decaying, in our case we considered α-functions.

In particular, we are interested in selecting model parameters for which uniformly distributed inputs $I = \{I_i\}$, where $I_i \in [V_{th}, V_{th} + \Delta V]$, produce cell assembly-like sequential patterns in the network. The main aspects of the desired activity can be summarized as follows: (i) single neurons should exhibit large variability in firing rates ($CV > 1$); (ii) the dynamical evolution of neuronal assemblies should reveal strong correlation within an assembly and anti-correlation with neurons out of the assembly. As suggested by many authors [10, 28] the dynamics of MSNs cannot be explained in terms of a *winners take all* (WTA) mechanism, which would imply a small number of highly firing neurons, while the remaining would be silenced. Therefore we will search, in addition to the requirements (i) and (ii), for a regime where a substantial fraction of neurons are actively involved in the network dynamics. This represents a third criterion (iii) to be fulfilled to obtain a striatum-like dynamical evolution.

Fig. 1 shows an example of such dynamics for the LIF model, with three pertinent similarities to previously observed dynamics of real MSN networks [12]. Firstly, cells are organized into correlated groups, and these groups are mutually anticorrelated (as evident from the cross-correlation matrix of the firing rates reported in Fig. 1 (c)). Secondly, individual cells within groups show irregular firing as shown in Fig. 1 (a). This aspect is reflected in a coefficient of variation (CV) of the inter-spike-intervals (ISIs) definitely greater than one (see the black curve in Fig. 3 (b)) as observed experimentally for the dynamics of rat striatum *in-vitro* [8, 10]. Thirdly, the raster plot reported in Fig. 1 (b) reveals that a large fraction of neurons (namely,$\simeq 93$ %) is actively involved in the neural dynamics.

A novel metric for the structured cell assembly activity

The properties (i),(ii), and (iii), characterizing MSN activity, can be quantified in terms of a single scalar metric Q_0, as follows:

$$Q_0 \equiv \langle CV \rangle_N \times \sigma(C(\nu_i, \nu_j)) \times n^* \quad ; \tag{1}$$

where $\langle \cdot \rangle_N$ denotes average over the ensemble of N neurons, $n^* = N_{act}/N$ is the fraction of active neurons N_{act} out of the total number, $C(\nu_i, \nu_j)$ is the $N \times N$ zero-lag cross-correlation matrix between all the pairs of single neuron firing rates (ν_i, ν_j), and $\sigma(\cdot)$ is the standard deviation of this matrix (for details see Methods). We expect that good parameter values for our model can be selected by maximizing Q_0.

Our metric is inspired by a metric introduced to identify the level of cluster synchronization and organization for a detailed striatal microcircuit model [29]. However, that metric is based on the similarity among the point-process spike trains emitted by the various neurons, whereas Q_0 uses correlations between firing rate time-courses. Furthermore, Q_0 takes also in account the variability of the firing rates, by including the average CV in Eq. (1), an aspect of the MSN dynamics omitted by the metric employed in [29]. Within biologically meaningful ranges, we find values of the parameters controlling lateral inhibition (namely, the synaptic strength g and the the post-synaptic potential duration τ_α) that maximize Q_0. As we show below, the chosen parameters not only produce MSN-like network dynamics but also optimize the network′s computational capabilities, in the sense of producing a consistent, temporally-structured response, to a given pattern of inputs while discriminating between inputs which differ only for a few elements.

The role of lateral inhibition

In this sub-section we examine how network dynamics is affected by the strength of inhibitory connections (Fig. 2). When these lateral connections are very weak (parameter g close to zero), the dominant input to each neuron is the constant excitation. As a result, most individual neurons are active (fraction of active neurons, n^*, is close to 1) and firing regularly (CV close to zero). As lateral inhibition is made stronger, some neurons begin to slow down or even stop firing, and n^* declines towards a minimum fraction of $\simeq 50\%$ (at $g = g_{min}$). As noted by Ponzi and Wickens [17], this is due to a winner-take-all (WTA) mechanism : faster-firing neurons depress or even silence the neurons to which they are connected. This is evident from the distribution $P(\overline{ISI})$ of the average interspike intervals ($\overline{ISI}$), which is peaked at low firing periods, and from the distribution of the CV exhibiting a single large peak at $CV \simeq 0$ (as shown in the insets of Figs. S2 (a,b) and (d,e)).

As soon as $g > g_{min}$, the neuronal activity is no longer due only to the *winners*, but also the *losers* begin to play a role. The *winners* are characterized by an effective input W_i which is on average supra-threshold, while their firing activity is driven by the mean current: *winners* are *mean-driven* [30]. On the other hand, *losers* are on average below-threshold, and their firing is due to current fluctuations: *losers* are *fluctuation-driven* [30]. For more details see Figs. S2 (c) and (f)). This is reflected in the corresponding distribution $P(\overline{ISI})$ (Fig. 2(b), red curve). The *winners* have very short $\overline{ISI}$s (i.e. high firing rates), while the *losers* are responsible for the long tail of the distribution extending up to $\overline{ISI} \simeq 10^3$ s. In the distribution of the coefficients of variation (Fig. 2(b) inset, red curve) the *winners* generate a peak of very low CV (i.e. highly-regular firing), suggesting that they are not strongly influenced by the other neurons in the network and therefore have an effective input on average supra-threshold. By contrast the *losers* are associated with a smaller peak at $CV \simeq 1$, confirming that their firing is due to large fluctuations in the currents.

Counterintuitively however, further increases in lateral inhibition strength result in increased neuronal participation, with n^* progressively returning towards $\simeq 1$. The same effect was previously reported by Ponzi and Wickens [17] for a different, more complex, model. When the number of active neurons returns almost to 100%, i.e. for sufficiently large coupling $g > g_{min}$, most of the neurons appear to be below threshold, as revealed by the distribution of the effective inputs W_i reported in Figs. S2 (c) and (f). Therefore in this case the network firing is essentially fluctuation-driven, as a matter of fact the $P(\overline{ISI})$ distribution is now characterized by a broader distribution and by the absence of the peak at short $\overline{ISI}$ (as shown in Fig. 2 (b), blue line; see also Figs. S2(a) and (d)). Furthermore the single neuron dynamics is definitely bursting, as shown by the fact that the CV distribution is now centered around $CV \simeq 2$ (inset of Fig. 2 (b), blue line; see also Figs. S2(b) and (e)).

The transition between the two dynamical regimes, occurring at $g = g_{min}$, is due to a passage from a state where some *winner* neuron were mean-driven and were able to depress all the other neurons, to a state at $g >> g_{min}$ where almost all neurons are fluctuation-driven and contribute to the network activity. The transition occurs because at $g < g_{min}$ the fluctuations in the effective input currents W_i are small and insufficient to drive the *losers* towards the firing threshold (as shown in the insets of Fig. S2 (c) and (f)). At $g \simeq g_{min}$ the amplitude of the fluctuations becomes sufficient for some *losers* to cross the firing threshold and contribute to the number of active neurons. This will also reduce the *winners'* activity. For $g >> g_{min}$ the fluctuations of W_i are sufficient to lead almost all *losers* to fire and no clear distinction between *losers* and *winners* remains. The transition is due to the fact that not only the average inhibitory action is proportional to the synaptic strength, but also the amplitude of the current fluctuations increases linearly with g, at least for $g > g_{min}$ (as shown in Figs. S3(a) and (b) and explained in Text S1).

The reported results explain why the variability $\sigma(C)$ of the cross-correlation matrix has a non monotonic behaviour with g (as shown in the middle panel in Fig. 2(a)). At low coupling $\sigma(C)$ is almost zero, since the single neuron dynamics are essentially independent one from another, while the increase of the coupling leads to an abrupt rise of $\sigma(C)$. This growth is clearly associated with the inhibitory action which splits the neurons into correlated and anti-correlated groups. The variability of the cross-correlation matrix achieves a maximum value for coupling slightly larger than g_{min}, where fluctuations in the effective currents begin to play a relevant role in the network dynamics. At larger coupling $\sigma(C)$ begins to decay towards a finite non zero value. These results confirm that the most interesting region to examine is the one with coupling $g > g_{min}$, as already suggested in [17].

The observed behaviour of CV, n^* and $\sigma(C)$ suggests that we should expect a maximum in Q_0 at some intermediate coupling $g > g_{min}$, as indeed we have found for both studied cases, as shown in Fig. 2 (c) and (d). The initial increase in Q_0 is due to the increase in CV and n^*, while the final decrease, following the occurrence of the maximum, is essentially driven by the decrease of $\sigma(C)$. For larger ΔV the neurons tend to fire regularly in a wider range of coupling at small g (see Fig. 2 (d)), indicating that due to their higher firing rates a larger synaptic inhibition is required to influence their dynamics. On the other hand, their bursting activity observable at large g is more irregular (see the upper panel in Fig. 2 (a); dashed line and empty symbols).

To assess whether parameters that maximize Q_0 also allow discrimination between different inputs, we alternated the network back and forth between two distinct input patterns, each presented for a period T_{sw}. During this stimulation

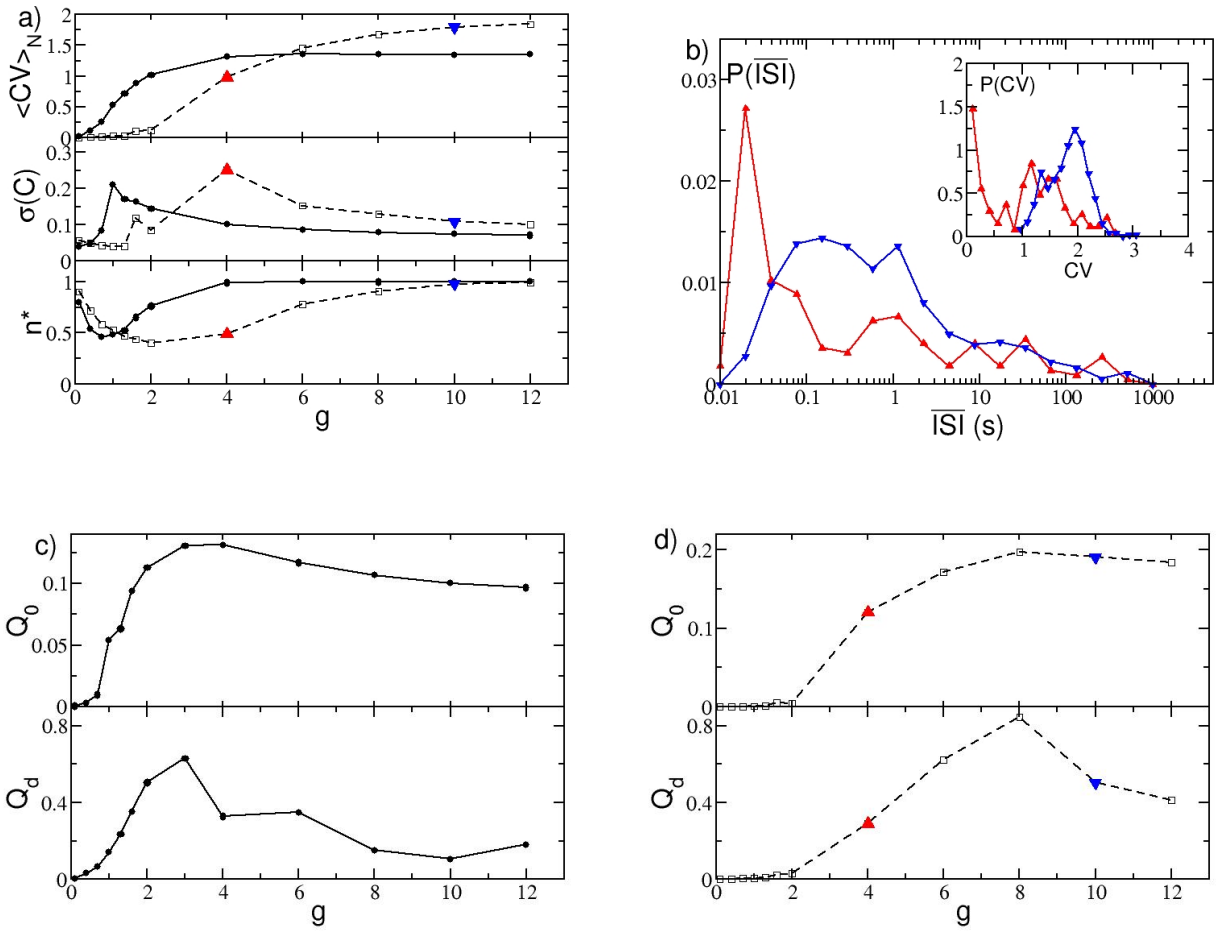

FIG. 2. **Metrics of structured activity vs lateral inhibition strength.** a) Metrics entering in the definition of Q_0 versus the synaptic strength g. From top to bottom: Averaged coefficient of variation $\langle CV \rangle_N$, standard deviation of the cross-correlation matrix $\sigma(C)$, and the fraction of active neurons n^*. The solid (dashed) line refers to the case $\Delta V = 1$ mV ($\Delta V = 5$ mV). The minimum number of active neurons is achieved at $g = g_{min}$, this corresponds to a peak amplitude of the PSP $A_{PSP} = 0.064$ mV ($A_{PSP} = 0.184$ mV) for $\Delta V = 1$ mV ($\Delta V = 5$ mV) (for more details see Methods). b) Distributions $P(\overline{ISI})$ of the average ISI for a fixed $\Delta V = 5$ mV and for two different coupling strengths, $g = 4$ (red triangle-up symbol) and $g = 10$ (blue triangle-down). Inset, the distribution $P(CV)$ of the CV of the single neurons for the same two cases. c) Q_0 and Q_d, as defined in Eqs. (1) and (15), versus g for $\Delta V = 1$ mV. d) Same as c) for $\Delta V = 5$ mV. Other parameters as in Fig. 1

protocol, we evaluated the state transition matrix (STM) and the associated quantity ΔM_d. The STM measures the similarity among the firing rates of the neurons in the network taken at two different times. The metric ΔM_d, based on the STM, has been introduced in [17] to quantify the ability of the network to distinguish between two inputs. In particular, ΔM_d is the difference between the average values of the STM elements associated with the presentation of each of the two stimuli (a detailed description of the procedure is reported in the sub-section *Discriminative and computation capability* and in Methods).

To verify whether the ability of the network to distinguish different stimuli is directly related to the presence of dynamically correlated and anti-correlated cell assemblies, we generated a new metric, Q_d. This metric is defined in the same way as Q_0, except that in in Eq. (1) the standard deviation of the correlation matrix is replaced by ΔM_d. As it can be appreciated from Figs. 2(c) and 2(d) the metrics Q_d and Q_0 behave similarly, indicating that indeed Q_0 becomes maximal in the parameter range in which the network is most effectively distinguishing different stimuli. We speculate that the emergence of correlated and anti-correlated assemblies contributes to this discriminative ability.

We note that we observed maximal values of Q_0 for realistic lateral inhibition strengths, as measured from the post-synaptic amplitudes A_{PSP}. Specifically, Q_0 reaches the maximum at $g = 4$ ($g = 8$) for $\Delta V = 1$ mV ($\Delta V = 5$ mV) corresponding to $A_{PSP} = 0.368$ mV ($A_{PSP} = 0.736$ mV), comparable to previously reported experimental results [8, 10, 28] (for more details see Methods).

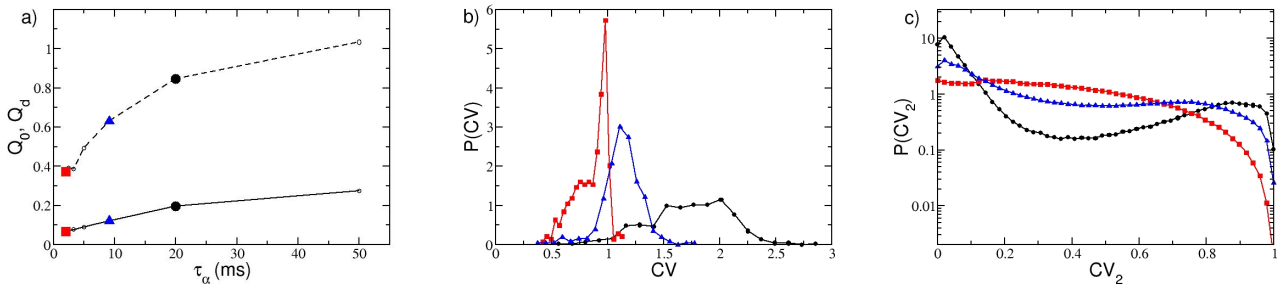

FIG. 3. **Metrics of structured activity vs post-synaptic time duration.** a) Metrics Q_0 (in solid line) and Q_d (dashed) as a function of the pulse time scale for the parameter values $\{\Delta V, g\} = \{5\ \text{mV}, 8\}$ corresponding to the maximum Q_0 value in Fig. 2(d). Probability distribution functions $P(CV)$ ($P(CV_2)$) for the coefficient of variation CV (local coefficient of variation CV_2) are shown in b) (in c)) for three representative $\tau_\alpha = \{2, 9, 20\}$ ms, displayed by employing the same symbols and colors as indicated in a). For these three cases the average firing rate in the network is $\langle\nu\rangle = \{8.81, 7.65, 7.35\}$ Hz ordered for increasing τ_α-values. Other parameters as in Fig. 1

The role of the post-synaptic time scale

In brain slice experiments IPSCs/IPSPs between MSNs last 5-20 ms and are mainly mediated by the $GABA_a$-receptor [8, 31]. In this sub-section, we will examine the effect of the the post-synaptic time constant τ_α. As τ_α is increased from 2 to 50 ms, the values of of both metrics Q_0 and Q_d progressively increase (Fig. 3(a)), with the largest variation having already occurred by $\tau_\alpha = 20$ ms. To gain more insights on the role of the PSP in shaping the structured dynamical regime, we show for the same network the distribution of the single cell CV, for $\tau_\alpha = \{2, 9, 20\}$ ms (Fig. 3(b)). Narrow pulses ($\tau_\alpha \simeq 2$ ms) are associated with a distribution of CV values ranging from 0.5 to 1, with a predominant peak at one. By increasing τ_α one observes that the CV distributions shift to larger and larger CV values. Therefore, one can conclude that at small τ_α the activity is mainly Poissonian, while increasing the duration of the PSPs leads to bursting behaviours, as in experimental measurements of the MSN activity [22]. In particular in [22], the authors showed that bursting activity of MSNs with a distribution $P(CV)$ centered around $CV \simeq 2$ is typical of awake wild-type mice. To confirm this analysis we have estimated also the distribution of the CV_2: A CV_2 distribution with a peak around zero denotes a very regular firing, while a peak around one indicates the presence of long silent periods followed by rapid firing events (i.e. a bursting activity). Finally a flat distribution denotes Poissonian distributed spiking. It is clear from Fig. 3(c) that by increasing τ_α from 2 to 20 ms this leads the system from an almost Poissonian behaviour to bursting dynamics, where almost regular firing inside the burst (intra-burst) is followed by a long quiescent period (inter-burst) before starting again.

The distinct natures of the distributions of CV for short and long-tailed pulses raises the question of what mechanism underlies such differences. To answer this question we analyzed the distribution of the ISI of a single cell in the network for two cases: in a cell assembly bursting regime (corresponding to $\tau_\alpha = 20$ ms) and for Poissonian unstructured behavior (corresponding to $\tau_\alpha = 2$ ms). We expect that even the single neurons should have completely different dynamics in these two regimes, since the distributions $P(CV)$ at $\tau_\alpha = 2$ ms and 20 ms are essentially not overlapping, as shown in Fig. 3(b). In order to focus the analysis on the effects due to the synaptic inhibition, we have chosen, in both cases, neurons receiving exactly the same external excitatory drive I_s. Therefore, in absence of any synapses, these two neurons will fire with the same period $\text{ISI}_0 = \tau_m \log[(I_s - V_r)/(I_s - V_{th})] = 12$ ms, corresponding to a firing rate of 8.33 Hz not far from the average firing rate of the networks (namely, $\langle\nu\rangle_N \simeq 7 - 8$ Hz). Thus these neurons can be considered as displaying a typical activity in both regimes. As expected, the dynamics of the two neurons is quite different, as evident from the $P(ISI)$ presented in Fig. 4(a) and (b). In both cases one observes a long tailed exponential decay of $P(ISI)$ corresponding to a Poissonian like behaviour. However the decay rate ν_D is slower for $\tau_\alpha = 20$ ms with respect to $\tau_\alpha = 2$ ms, namely $\nu_D \simeq 2.74$ Hz versus $\nu_D \simeq 20.67$ Hz. Interestingly, the main macroscopic differences between the two distributions arises at short time intervals. For $\tau_\alpha = 2$ ms, (see Fig. 4(b)) an isolated and extremely narrow peak appears at ISI_0. This first peak corresponds to the supra-threshold tonic-firing of the isolated neuron, as reported above. After this first peak, a gap is clearly visible in the $P(ISI)$ followed by an exponential tail. The origin of the gap resides in the fact that $\text{ISI}_0 >> \tau_\alpha$, because if the neuron is firing tonically with its period ISI_0 and receives a single PSP, the membrane potential has time to decay almost to the reset value V_r before the next spike emission. Thus a single PSP will delay the next firing event by a fixed amount corresponding to the gap in Fig. 4(b). Indeed one can estimate analytically this delay due to the arrival of a single α-pulse, in the

present case this gives $\mathrm{ISI}_1 = 15.45$ ms, in very good agreement with the results in Fig. 4(b). No further gaps are discernible in the distribution, because it is highly improbable that the neuron will receive two (or more) PSPs exactly at the same moment at reset, as required to observe further gaps. The reception of more PSPs during the ramp up phase will give rise to the exponential tail in the $P(ISI)$. In this case the contribution to the CV comes essentially from this exponential tail, while the isolated peak at ISI_0 has a negligible contribution.

On the other hand, if $\tau_\alpha > \mathrm{ISI}_0$, as in the case reported in Fig. 4(a), $P(ISI)$ does not show anymore a gap, but instead a continuous distribution of values. This because now the inhibitory effects of the received PSPs sum up leading to a continuous range of delayed firing times of the neuron. The presence of this peak of finite width at short ISI in the $P(ISI)$ plus the exponentially decaying tail are at the origin of the observed $CV > 1$. In Fig. 4 (e) and 4 (f) the distributions of the coefficient $CV_2^{(i)}$ are also displayed for the considered neurons as black lines with symbols. These distributions clearly confirm that the dynamics are bursting for the longer synaptic time scale and essentially Poissonian for the shorter one.

We would like to understand whether it is possible to reproduce similar distributions of the ISIs by considering an isolated cell receiving Poissonian distributed inhibitory inputs. In order to verify this, we simulate a single cell receiving K uncorrelated spike trains at a rate $\langle\nu\rangle_N$, or equivalently, a single Poissonian spike train with rate $K\langle\nu\rangle_N$. Here, $\langle\nu\rangle_N$ is the average firing rate of a single neuron in the original network. The corresponding $P(ISI)$ are plotted in Fig. 4 (c) and 4 (d), for $\tau_\alpha = 20$ ms and 2 ms, respectively. There is a remarkable similarity between the reconstructed ISI distributions and the real ones (shown in Fig. 4(a) and (b)) , in particular at short ISIs. Also the distributions of the $CV_2^{(i)}$ for the reconstructed dynamics are similar to the original ones, as shown in Fig. 4 (e) and 4 (f). Altogether, these results demonstrate that the bursting activity of inhibitory coupled cells is not a consequence of complex correlations among the incoming spike trains, but rather a characteristic related to intrinsic properties of the single neuron: namely, its tonic firing period, the synaptic strength, and the post-synaptic time decay. The fundamental role played by long synaptic time in inducing bursting activity has been reported also in a study of a single LIF neuron below threshold subject to Poissonian trains of exponentially decaying PSPs [32].

Obviously this analysis cannot explain collective effects, like the non trivial dependence of the number of active cells n^* on the synaptic strength, discussed in the previous sub-section, or the emergence of correlations and anti-correlations among neural assemblies (measured by $\sigma(C)$) due to the covarying of the firing rates in the network, as seen in the striatum slices and shown in Fig. 1 (c) for our model. To better investigate the influence of τ_α on the collective properties of the network we report in Fig. S5(a) and (b) the averaged CV, $\sigma(C)$, n^* and ΔM_d for $\tau_\alpha \in [2, 50]$ ms. As already noticed, the network performs better in mimicking the MSN dynamics and in discriminating between different inputs at larger τ_α (e.g. at 20 ms). However, what is the minimal value of τ_α for which the network still reveals cell assembly dynamics and discriminative capabilities ? From the data shown in Fig. S5(a) one can observe that $\sigma(C)$ and ΔM_d attain their maximal values in the range 10 ms $\leq \tau_\alpha \leq$ 20 ms. This indicates that clear cell assembly dynamics with associated good discriminative skills can be observed in this range. However, the bursting activity is not particularly pronounced at $\tau_\alpha = 10$ ms, where $\langle CV\rangle_N \simeq 1$. Therefore only the choice $\tau_\alpha = 20$ ms fulfills all the requirements.

Interestingly, genetic mouse models of Huntington's disease (HD) revealed that spontaneuous IPSCs in MSNs has a reduced decay time and half-amplitude duration compared to wild-types [21]. Our analysis clearly indicate that a reduction of τ_α results in more stochastic single-neuron dynamics, as indicated by $\langle CV\rangle_N \simeq 1$, as well as in a less pronounced structured assembly dynamics (Fig. S5 (a)). This resembles what observed for the striatum dynamics of freely behaving mice with symptomatic HD [22]. In particular, the authors have shown in [22] that at the single unit level HD mice reveals a $CV \simeq 1$ in contrast to $CV \simeq 2$ for wild-type mice, furthermore the correlated firing was definitely reduced in HD mice.

Structural origin of the cell assemblies

A question that we have not addressed so far is: how do cell assemblies arise ? Since the network is purely inhibitory it is reasonable to guess that correlation (anti-correlation) among groups of neurons will be related to the absence (presence) of synaptic connections between the considered groups. In order to analyze the link between the correlation and the network connectivity we compare the clustered cross-correlation matrix of the firing rates $C(\nu_i, \nu_j)$ (shown in Fig 5 (a)) with the associated connectivity matrix $\mathcal{C}_{ij}$ (reported in Fig- 5 (b)). The cross-correlation matrix is organized in $k = 15$ clusters via the *k-means* algorithm, therefore we obtain a matrix organized in a $k \times k$ block structure, where each block (m, l) contains all the cross-correlation values of the elements in cluster m with the elements in cluster l. The connectivity matrix is arranged in exactly the same way, however it should be noticed that while $C(\nu_i, \nu_j)$ is symmetric, the matrix $\mathcal{C}_{ij}$ is not symmetric due to the unidirectional nature of the synaptic connections. From a visual comparison of the two figures it is clear that the most correlated blocks are along the

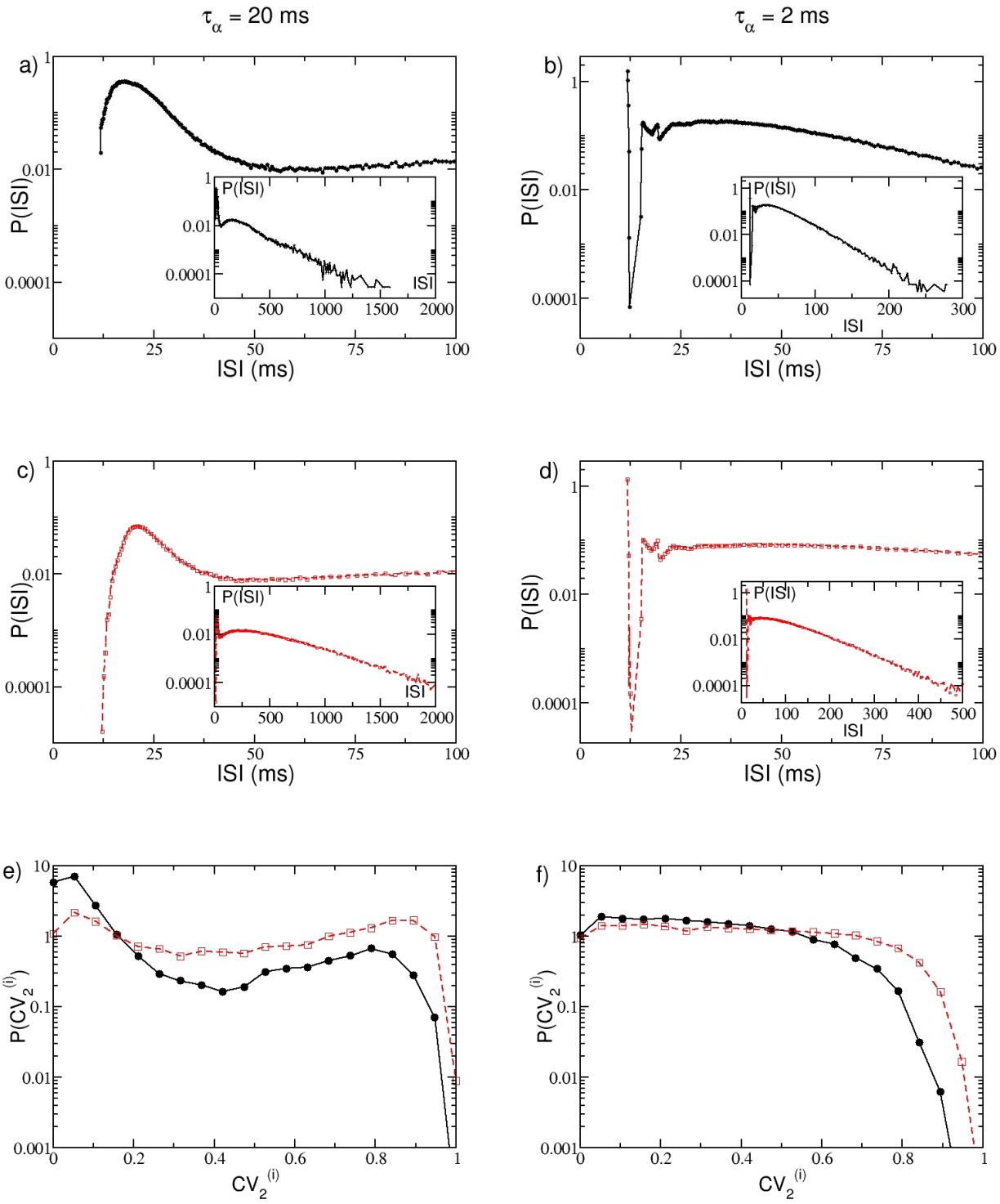

FIG. 4. **Single neuron statistics.** First row : distributions $P(ISI)$ for one representative cell in the network are shown in black. Second row: the corresponding Poissonian reconstruction of the $P(ISI)$ are reported in red. In all plots the main figure displays the distributions at short ISIs, while the inset is a zoom out of the whole distribution. Third row: single neuron distribution of the $CV_2^{(i)}$ for the considered neuron (black solid lines with circles) and its Poissonian distribution (red dashed line with squares). The left (right) column corresponds to $\tau_\alpha = 20$ (2 ms). The network parameters are $\Delta V = 5$ mV and $g = 8$, and the others as in Fig. 1, both the examined neurons have $I_s = -45.64$ mV. For the Poissonian reconstruction the frequencies of the incoming uncorrelated spike trains are set to $\langle\nu\rangle_N \approx 7.4$ Hz ($\langle\nu\rangle_N \approx 8.3$ Hz) for $\tau_\alpha = 20$ms ($\tau_\alpha = 2$ms), as measured from the corresponding network dynamics. The distributions are obtained by considering a sequence of 10^9 spikes in the original network, and 10^7 events for the Poissonian reconstruction.

diagonal and that the number of connections present in these diagonal blocks is definitely low, with respect to the expected value from the whole matrix. An exception is represented by the largest diagonal block which reveals, however, an almost zero level of correlation among its members. We have highlighted in blue some blocks with high level of anti-correlations among the elements, the same blocks in the connectivity matrix reveal a high number of links. A similar analysis, leading to the same conclusions was previously reported in [15].

However, we would like to make more quantitative this comparison. Therefore we have estimated for each block the average cross-correlation, denoted as $\langle C \rangle_{ml}$, and the average probability p_{ml} of unidirectional connections from the cluster l to the cluster m. These quantities are shown in Fig. 5 (c) for all the possible blocks, it is evident that the correlation $\langle C \rangle_{ml}$ decreases with the probability p_{ml}, a linear fit to the data is reported in the figure as a solid black line. However, there are blocks that are outliers with respect to this fit, in particular the black squares refer to the diagonal blocks and these are all associated to high correlation values $\langle C \rangle_{mm}$ and low probabilities p_{mm}, definitely smaller than the average probability $p = 0.05$, shown as a dashed vertical red line in Fig. 5 (c). An exception is represented by a single black square located exactly on the linear fit in proximity of $p = 0.05$, this is the large block with almost zero level of correlation among its elements previously identified. Furthermore, the blocks with higher anticorrelation, denoted as blue triangles in the figure, have probabilities p_{ml} definitely larger than 5 %. Also in this case there are 2 exceptions, 2 triangles lie exactly on the vertical dashed line corresponding to 5 %. This is due to the fact that the p_{ml} are not symmetric, and it is sufficient to have a large probability to have connections in only one of the two possible directions between blocks m and l to observe anti-correlated activities between the two assemblies. To summarize we have clearly shown that the origin of the assemblies dynamically identified from the correlations of the firing rates is directly related to structural properties of the networks, as visualized by the connectivity matrix.

Discriminative and computational capability

In this sub-section we examine the ability of the network to perform different tasks: namely, to respond in a reproducible manner to equal stimuli and to discriminate between similar inputs via distinct dynamical evolution. For this analysis we have always compared the responses of the network obtained for a set of parameters corresponding to the maximum Q_0 value shown in Fig. 2(d), where $\tau_\alpha = 20$ ms, and for the same parameters but with a shorter PSP decay time, namely $\tau_\alpha = 2$ ms.

To check for the capability of the network to respond to cortical inputs with a reproducible sequences of states of the network, we perform a simple experiment where two different inputs $I^{(1)}$ and $I^{(2)}$ are presented sequentially to the system. Each input persists for a time duration T_{sw} and then the stimulus is switched to the other one and this process is repeated for the whole simulation time. The raster plot measured during such an experiment is shown in Fig. 6 (a) for $\tau_\alpha = 20$ ms. Whenever one of the stimuli is presented, a specific sequence of pattern activations can be observed. Furthermore, the sequence of emerging activity patterns is reproducible when the same stimulus is again presented to the system, as can be appreciated by observing the patterns encircled with black lines in Fig. 6 (a). Recall that the clustering algorithm here employed to identify the different groups is applied only during the presentation of the first stimulus, therefore the sequential dynamics is most evident for that particular stimuli.

Furthermore, we can quantitatively calculate how similar is the firing activity in the network at different times by estimating the STM. The similarity is quantified by computing the normalized scalar product of the instantaneous firing rates of the N neurons measured at time t_i and t_j. We observe that the similarity of the activity at a given time t_0 and at a successive time $t_0 + 2mT_{sw}$ is high (with values between 0.5 and 0.75), thus suggesting that the response to the same stimulus is similar, while it is essentially uncorrelated with the response at times corresponding to the presentation of a different stimulus, i.e. at $t_0 + (2m-1)T_{sw}$ (since the similarity is always smaller than 0.4) (here, $m = 1, 2, 3...$). This results in a STM with a periodic structure of period T_{sw} with alternating high correlated blocks followed by low correlated blocks (see Fig. S6(b)). An averaged version of the STM calculated over a sequence of 5 presentations of $I^{(1)}$ and $I^{(2)}$ is shown in Fig. 6 (b) (for details of the calculation see Methods). These results show not only the capability of the network to distinguish between the stimuli, but also the reproducible nature of the system response. In particular, from Fig. 6 (b) it is evident how the patterns associated with the response to the stimulus $I^{(1)}$ or $I^{(2)}$ are clearly different and easily identifiable. We also repeated the numerical experiment for another different realization of the inputs, noticing essentially the same features previously reported (as shown in Fig. S6(a-c)). Furthermore, to test for the presence of memory effects influencing the network response, we performed a further test where the system dynamics was completely reset after each stimulation and before the presentation of the next stimulus. We do not observe any relevant change in the network response, so we can conclude that our results are robust.

Next, we examined the influence of the PSP time scale on the observed results. In particular, we considered the case $\tau_\alpha = 2$ ms, for this value the network does not reveal a large variability in the response showing a reduced number of patterns of activity. In particular, as shown in Fig. S6(d) it responds in a quite uniform manner during the presentation of each stimulus. Furthermore, the corresponding STM reported in Figs. S6(e) shows highly correlated

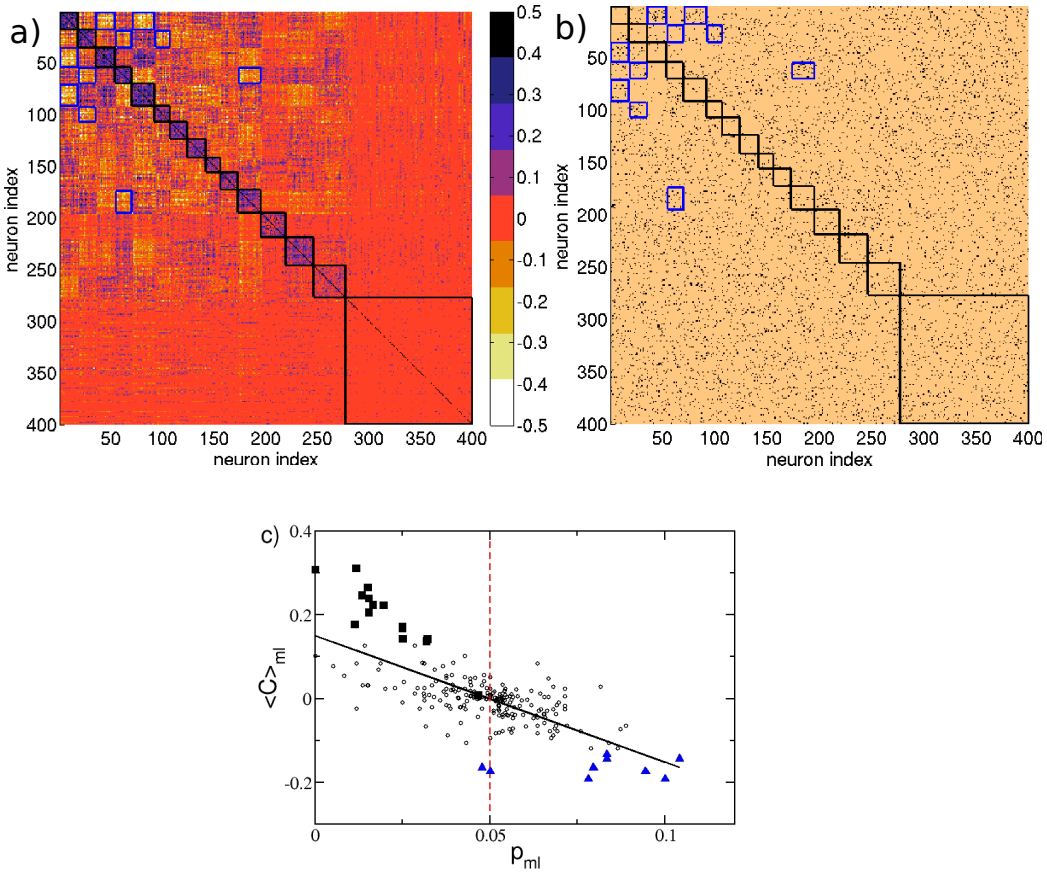

FIG. 5. **Cell assemblies and connectivity.** a) Cross-correlation matrix $C(\nu_i, \nu_j)$ of the firing rates organized according to the clusters generated via the *k-means* algorithm with $k = 15$, the clusters are ordered as in Fig. 1(c) from the highest to the lowest correlated one. b) Connectivity matrix $\mathcal{C}_{ij}$ with the indices ordered as in panel a). Here, a black (copper) dot denotes a 1 (0) in $\mathcal{C}_{ij}$, i.e. the presence of a synaptic connection from j to i. c) Average cross-correlation $\langle C \rangle_{ml}$ among the elements of the matrix block (m, l) , versus the probability p_{ml} to have synaptic connections from neurons in the cluster l to neurons in the cluster m. Black squares indicate the blocks along the diagonal delimited by black borders in panel a) and b) , i.e. they correspond to the pairs $\{\langle C \rangle_{mm}, p_{mm}\}$; blue triangles denote the ten blocks with the lowest $\langle C \rangle_{ml}$ values, which are also delimited by blue edges in a) and b). The vertical red dashed line indicates the average probability to have a connection $p = 5\%$. The black solid line is the linear regression to the data ($\langle C \rangle_{ml} \approx 0.15 - 3.02 p_{ml}$, correlation coefficient $R = -0.72$). Other parameters as in Fig. 1.

blocks alternating to low correlated ones, but these blocks do not reveal any internal structure typical of cell assembly encoding.

We proceeded to check the ability of the network to discriminate among similar inputs and how this ability depends on the temporal scale of the synaptic response. In particular, we tried to answer to the following question: if we present two inputs that differ only for a fraction f of the stimulation currents, which is the minimal difference between the inputs that the network can discriminate ? In particular, we considered a control stimulation $I^{(c)} = I_i \in [V_{th}, V_{th}+\Delta V]$ and a perturbed stimulation $I^{(p)}$, where the stimulation currents differ only over a fraction f of currents I_i (which are randomly chosen from the same distribution as the control stimuli). We measure the differences of the responses to the control and to the perturbed stimulations by measuring, over an observation window T_E, the dissimilarity metric $d^f(t)$, defined in Methods. The time averaged dissimilarity metric $\bar{d}^f$ is reported as a function of f in Fig. 7 for two different values τ_α. It is clear that for any f-value the network with longer synaptic response always discriminates better between the two different stimuli than the one with shorter PSP decay. We have also verified that the metric is robust to the modification of the observation times T_E, this is verified because the dissimilarity $d^f(t)$ rapidly reaches a steady value (as shown in Fig. S7(a) and (b)).

In order to better characterize the computational capability of the network and the influence due to the different duration of the PSPs, we measure the complexity of the output signals as recently suggested in [33]. In particular, we have examined the response of the network to a sequence of three stimuli, each being a constant vector of randomly

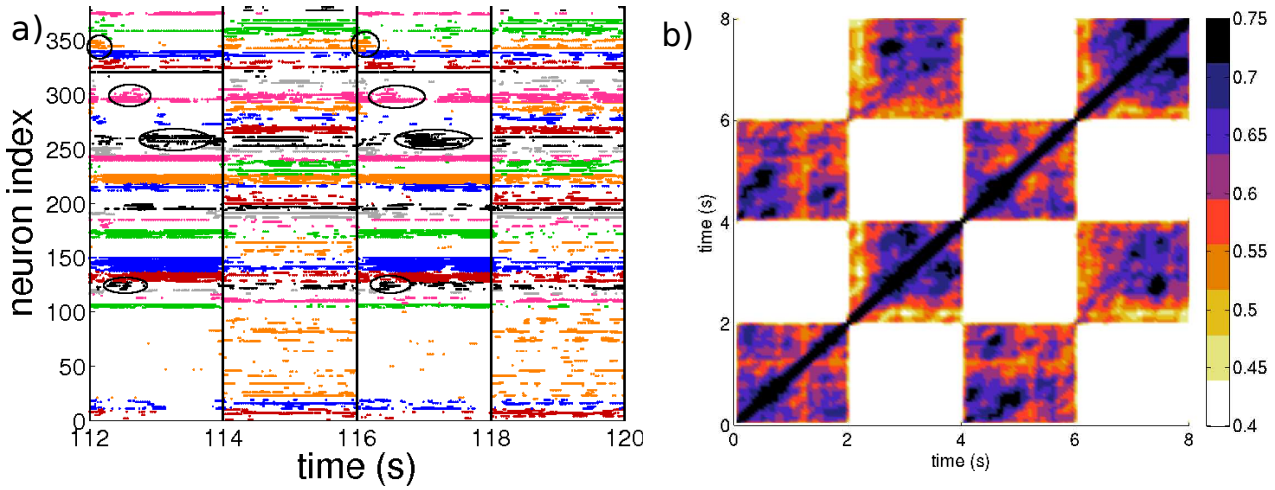

FIG. 6. **Sequential switching.** a) Raster plot associated to the two input protocols $I^{(1)}$ and $I^{(2)}$. The circles denote the clusters of active neurons appearing repetitively after the presentation of the stimulus $I^{(1)}$. Vertical lines denote the switching times between stimuli. b) Averaged State Transition Matrix $\overline{D}$, obtained by considering a $4T_{sw} \times 4T_{sw}$ sub-matrix averaged over $r = 5$ subsequent time windows of duration $4T_{sw}$ (see the section *Methods* for details). The inputs $I^{(1)}$ and $I^{(2)}$ are different realization of the same random process, they are obtained by selecting N current values I_i from the flat interval $[V_{th},\, V_{th}+\Delta V]$. The input stimuli are switched every $T_{sw} = 2$ s. Number of clusters $k = 35$ in a). Other parameters as in Fig. 1.

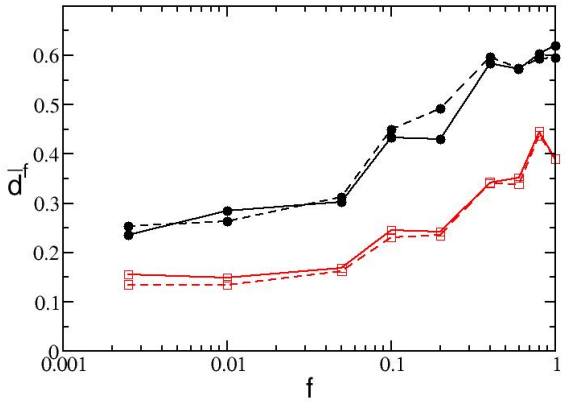

FIG. 7. **Pattern separation.** Average dissimilarity as a function of the fraction f of inputs differing from the control input, for the values of $\tau_\alpha = 20$ms (black circles) and $\tau_\alpha = 2$ms (red squares) with two different observation windows $T_E = 2$s (solid line) and $T_E = 10$s (dashed line). Other parameters used: $\Delta T = 50$ms, $\Delta V = 5$ mV. Remaining parameters as in Fig. 1.

chosen currents. The three different stimuli are consecutively presented to the network for a time period T_{sw}, and the stimulation sequence is repeated for the whole experiment duration T_E. The output of the network can be represented by the instantaneous firing rates of the N neurons measured over a time window $\Delta T = 100$ ms, this is a high dimensional signal, where each dimension is represented by the activity of a single neuron. The complexity of the output signals can be estimated by measuring how many dimensions are explored in the phase space, more stationary are the firing rates less variables are required to reconstruct the whole output signal [33].

A principal component analysis (PCA) performed over $T_E/\Delta T$ observations of the N firing rates reveals that for $\tau_\alpha = 2$ ms the 80% of the variance is recovered already with a projection over a two dimensional sub-space (red bars in Fig. 8 (a)). On the other hand, for $\tau_\alpha = 20$ ms a higher number of principal components is required to reconstruct the dynamical evolution (black bars in Fig. 8 (a)), thus suggesting higher computational capability of the system with longer PSPs [33].

These results are confirmed by analyzing the projections of the firing rates in the subspace spanned by the first

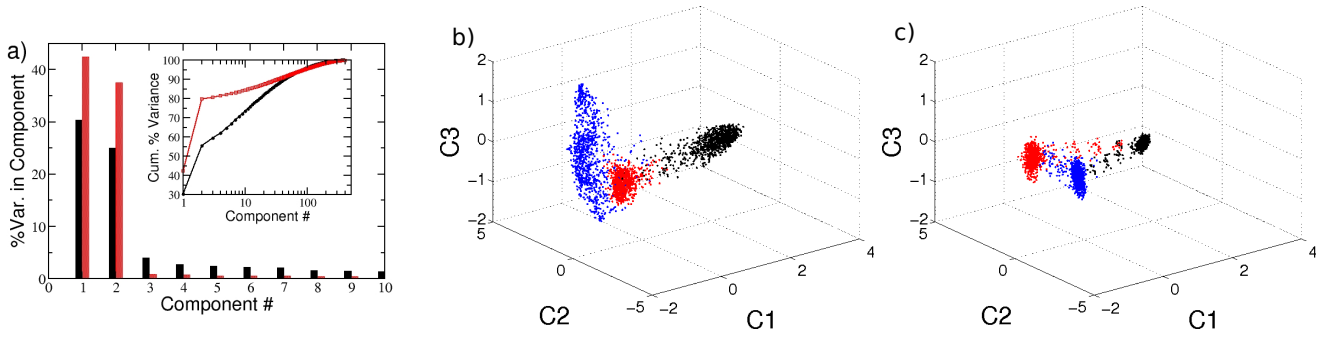

FIG. 8. **Computational capability of the network.** Characterization of the firing activity of the network, obtained as response to three consecutive inputs presented in succession. a) Percentage of the variance of the neuronal firing activity reproduced by each of the first 10 principal components. The inset displays the corresponding cumulative percentage as a function of the considered component. Filled black and shaded red (bar or symbols) correspond to $\tau_\alpha = 20$ ms and $\tau_\alpha = 2$ ms, respectively. Projection of the neuronal response along the first three principal components for b) $\tau_\alpha = 20$ ms and c) $\tau_\alpha = 2$ ms. Each point in the graph correspond to a different time of observation. The three colors denote the response to the three different inputs, which are constant stimulation currents randomly taken as $I^{(j)} \in [V_{th},\, V_{th} + \Delta V]$ for $j = 1, 2, 3$, the experiment is then performed as explained in the text.

three principal components $(C1, C2, C3)$ shown in Fig. 8 (b) and (c) for $\tau_\alpha = 20$ ms and $\tau_\alpha = 2$ ms, respectively. The responses to the three different stimuli can be effectively discriminated by both networks, since they lie in different parts of the phase space. However, the response to the three stimuli correspond essentially to three fixed points for $\tau_\alpha = 2$ ms, while trajectories evolving in a higher dimension are associated to each constant stimulus for $\tau_\alpha = 20$ ms.

These analyses confirm that the network parameters selected by employing the maximal Q_0 criterion also result in a reproducible response to different stimuli, as well as in an effective discrimination between different inputs.

In a recent work Ponzi and Wickens [17] have noticed that in their model the striatally relevant regimes correspond to marginally stable dynamical evolution. In the Supporting Information Text S1 we devote the sub-section *Linear stability analysis* to the investigation of this specific point, our conclusion is that for our model the striatally relevant regimes are definitely chaotic, but located in proximity of a transition to linearly stable dynamics. However for inhibitory networks it is known that even linearly stable networks can display erratic dynamics (resembling chaos) due to finite amplitude perturbations [34–37]. This suggests that the usual linear stability analysis, corresponding to the estimation of the maximal Lyapunov exponent [38], is unable to distinguish between regular and irregular evolution, at least for the studied inhibitory networks [37].

Physiological relevance for biological networks under different experimental conditions

The analysis here reported has been inspired by the experiment performed by Carrillo *et al.* [12]. In that experiment the authors considered a striatal network *in vitro*, which displays sporadic and asynchronous activity under control conditions. To induce spatio-temporal patterned activity they perfused the slice preparation with N-methyl-D-aspartate (NMDA). Since it is known that NMDA administration brings about an excitatory tonic drive with recurrent bursting activity [39, 40]. The crucial role of the synaptic inhibition in shaping the patterned activity in striatal dynamics is also demonstrated in [12], by applying the $GABA_a$ receptor antagonist bicuculline to effectively decrease the inhibitory synaptic effect.

In our simple model, ionic channels and NMDA-receptors are not modeled; nevertheless it is possible to partly recreate the effect of NMDA administration by increasing the excitability of the cells in the network, and the effect of the bicuculline as an effective decrease in the synaptic strength. We then verify *at posteriori* whether these assumptions lead to results similar to those reported in [12].

In our model the single cell excitability is controlled by the parameter I_i. The computational experiment consists in setting the system in a low firing regime corresponding to the control conditions with $I^{(c)} = \{I_i^{(c)}\} \in [-53, -49.5]$ mV and in enhancing, after 20 seconds, the system excitability to the range of values $I^{(e)} = \{I_i^{(e)}\} \in [-60, -45]$ mv, for another 20 seconds. This latter stage of the numerical experiment corresponds to the NMDA bath in the brain slice experiment. The process is repeated several times and the resulting raster plot is coarse grained as explained in Methods (sub-section *Synchronized Event Transition Matrix*).

From the coarse grained version of the raster plot, we calculate the *Network Bursting Rate* (NBR) as the fraction of neurons participating in a burst event in a certain time window. Whenever the instantaneous NBR is larger than the average NBR plus two standard deviations, this is identified as a *synchronized bursting event* (as shown in Fig. 9(a) and (f)). In Fig. 9(b) we plot all the neurons participating in a series of $S_s = 20$ synchronized bursting events. Here the switching times between control conditions and the regimes of increased excitability are marked by vertical dashed lines. Due to the choice of the parameters, the synchronized events occur only during the time intervals during which the network is in the enhanced excitability regime. Each synchronized event is encoded in a binary N dimensional vector $W_s(t)$ with 1 (0) entries indicating that the corresponding neuron was active (inactive) during such event. We then measure the similarity among all the events in terms of the *Synchronized Event Transition Matrix* (SETM) shown in Fig. 9(c). The SETM is the normalized scalar product of all pairs of vectors W_s registered in a given time interval (for more details see Methods). Furthermore, using the SETM we divide the synchronized events into clusters according to an optimal clustering algorithm [41] (see Methods). In the present case we have identified 3 distinct *states* (clusters), if we project the vectors W_s, characterizing each single synchronized event, on the two dimensional space spanned by the first two principal components $(C1, C2)$, we observe a clear division among the 3 states (see Fig. 9(d)). It is now important to understand whether the cells firing during the events classified as a state are the same or not. We observe that the groups of neurons recruited for each synchronized event, corresponding to a certain state, largely overlap, while the number of neurons participating to different states is limited. As shown in Fig. 9(e), the number of neurons participating to the events associated to a certain state is of the order of 40-50, while the coactive neurons (those participating in more than one state) ranges from 12 to 25. Furthermore, we have a core of 9 neurons which are firing in all states. Thus we can safely identify a distinct assembly of neurons active for each state.

As shown in Fig. 9(c), we observe, in analogy to [12], that the system alternates its activity among the previously identified cell assemblies. In particular, we have estimated the transition probabilities from one state to any of the three identified states. We observe that the probability to remain in state 2 or to arrive to this state from state 1 or 3 is quite high, ranging between 38 and 50 %, therefore this is the most visited state. The probability that two successive events are states of type 1 or 2 is also reasonably high ranging from $\simeq 29 - 38\%$ as well as the probability that from state 1 one goes to 2 or viceversa ($\simeq 38 - 43\%$). Therefore the synchronized events are mostly of type 1 and 2, while the state 3 is the less *attractive*, since the probability of arrving to this state from the other ones or to remain on it once reached, are between 25 - 29 %. If we repeat the same experiment after a long simulation interval $t \simeq 200$ s we find that the dynamics can be always described in terms of small number of states (3-4), however the cells contributing to these states are different from the ones previously identified. This is due to the fact that the dynamics is in our case chaotic, as we have verified in the Supporting Information Text S1 (*Linear Stability Analysis*). Therefore even small differences in the initial state of the network, can have macroscopic effects on sufficiently long time scales.

To check for the effect of bicuculline, the same experiment is performed again with a much smaller synaptic coupling, namely $g = 1$, the results are shown in Fig. 9(f-j). The first important difference can be identified in higher NBR values with respect to the previous analyzed case ($g = 8$) Fig. 9(f). This is due to the decreased inhibitory effect, which allows most of the neurons to fire almost tonically, and therefore a higher number of neurons participate in the bursting events. In Fig. 9(g) it is clearly visible a highly repetitive pattern of synchronized activity (identified as state 2, blue symbols), this state emerges immediately after the excitability is enhanced. After this event we observe a series of bursting events, involving a large number of neurons (namely, 149), which have been identified as an unique cluster (state 1, red symbols). The system, analogously to what shown in [12], is now locked in an unique state which is recurrently visited until the return to control conditions. Interestingly, synchronized events corresponding to state 1 and state 2 are highly correlated when compared with the $g = 8$ case, as seen by the SETM in Fig. 9(h). Despite this, it is still possible to identify both states when projected on the two dimensional space spanned by the first two principal components (see Fig. 9(i)). This high correlation can be easily explained by the fact that the neurons participating in state 2 are a subset of the neurons participating in state 1, as shown in Fig. 9(j). Furthermore, the analysis of the transition probabilities between states 1 and 2 reveals that starting from state 2 the system never remains in state 2, but always jumps to state 1. The probability of remaining in state 1 is really high $\simeq 64\%$. Thus we can affirm that in this case the dynamics is really dominated by the state 1.

To determine the statistical relevance of the results presented so far, we repeated the same experiment for ten different random realizations of the network, the detailed analysis of two of these realizations is reported in Figs. S8(a-h) (see also Text S1). We found that, while the number of identified states may vary from one realization to another, the persisting characteristics that distinguish the NMDA perfused scenario and the decreased inhibition one, are the variability in the SETM and the fraction of coactive cells. More precisely, on one hand the average value of the elements of the SETM is smaller for $g = 8$ with respect to the $g = 1$ case, namely 0.54 versus 0.84, on the other hand their standard deviation is larger, namely 0.15 versus 0.07. Thus indicating that the states observed with $g = 1$ are much more correlated among them with respect to the states observable for $g = 8$, which show a larger variability. The analysis of the neurons participating to the different states revealed that the percentage of neurons coactive in

the different states passes from 51 % at $g = 8$ to 91 % at $g = 1$. Once more the reduction of inhibition leads to the emergence of states which are composed by almost the same group of active neurons, representing a dominant state. These results confirm that inhibition is fundamental to cell assembly dynamics.

Altered intrastriatal signaling has been implicated in several human disorders, and in particular there is evidence for reduced GABAergic transmission following dopamine depletion [42], as occurs in Parkinson's disease. Our simulations thus provide a possible explanation for observations of excessive entrainment into a dominant network state in this disorder [23, 43].

III. DISCUSSION

In summary, we have shown that lateral inhibition is fundamental for shifting the network dynamics from a situation where a few neurons, tonically firing at a high rate, depress a large part of the network, to a situation where all neurons are active and fire with similar slow rates. In particular, if inhibition is too low, or too transient, *winner takes all* mechanism is at work and the activity of the network is mainly mean-driven. By contrast, if inhibition has realistic strength and duration, almost all the neurons are on average sub-threshold and the dynamical activity is fluctuation-driven [30].

Therefore we can reaffirm that the MSN network is likely capable of producing slow, selective, and reproducible activity sequences as a result of lateral inhibition. The mechanism at work is akin to the *winerless competition* reported to explain the functioning of olfactory networks in order to discriminate different odors [44]. Winnerless competition refers to a dynamical mechanism, initially revealed in asymmetrically coupled inhibitory rate models [45], displaying a transient slow switching evolution along a series of metastable saddles (for a recent review on the subject see [46]). In our case, the sequence of metastable states can be represented by the firing activity of the cell assembly, switching over time. In particular, as in our analysis, slow synapses have been recognized as a fundamental ingredient, besides asymmetric inhibitory connections, to observe the emergence of winnerless competition in realistic neuronal models [47, 48].

We have introduced a new metric to encompass in a single indicator key aspects of this patterned sequential firing, and with the help of this metric we have identified the values of the parameters entering in the model to best obtain these dynamics. Furthermore, for the same choice of parameters the network is able to respond in a reproducible manner to the same stimulus, presented at different times, while presenting complex computational capability by responding to constant stimuli with an evolution in a high dimensional space [33].

Our analysis has revelealed that the IPSP/IPSC duration is crucial in order to observe bursting dynamics at the single cell level as well as structured assembly dynamics at the population level. A reduction of the synaptic time has been observed in symptomatic HD mice [21], in our model this reduction leads single neurons towards a Poissonian behaviour and to a reduced level of correlation/anticorrelation among neural assemblies, in agreement with experimental results reported for mouse models of HD [22].

In summary, we have been able to reproduce general experimental features of MSN networks in brain slices [12]. In particular, we have observed, as in the experiment, a structured activity alternating among a small number of distinct cell assemblies. Furthermore, we have reproduced the dynamical effects induced by decreasing the inhibitory coupling: the drastic reduction of the inhibition leads to the emergence of a dominant highly correlated neuronal assembly. This may help account for the dynamics of Parkinsonian striatal microcircuits, where dopamine deprivation impairs the inhibitory feedback transmission among MSNs [23, 42]. Network models such as the one presented here offer a path towards understanding just how pathologies that affect single neurons lead to aberrant network activity patterns, as seen in Parkinson's and Huntington's diseases, and this is an exciting direction for future research.

IV. METHODS

The model

We considered a network of N LIF inhibitory neurons coupled via α pulses, which can be represented via the following set of $3N$ equations.

$$\dot{v}_i(t) = a_i - v(t) - gE_i(t) \tag{2a}$$

$$\dot{E}_i(t) = P_i(t) - \alpha E_i(t) \qquad\qquad i = 1, \ldots, N \tag{2b}$$

$$\dot{P}_i(t) = -\alpha P_i(t) + \frac{\alpha^2}{K} \sum_{n|t_n<t} \mathcal{C}_{i,j}\delta(t - t_n)\,. \tag{2c}$$

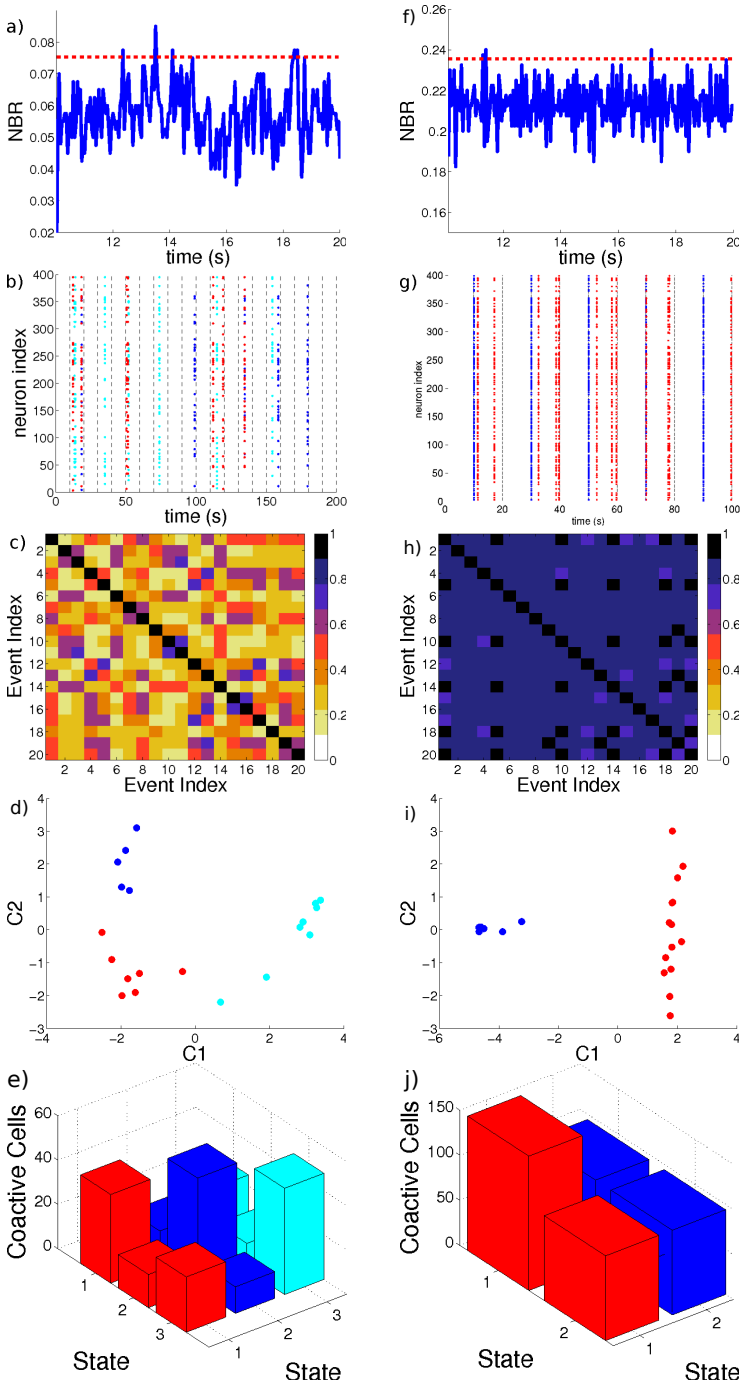

FIG. 9. **Response of the network to an increase in the excitability.** a,f) Network Bursting Rate, and the threshold defined for considering a synchronized event. b,g) Neurons involved in the synchronized events, vertical lines denoted the switching times between the excited $I^{(e)}$ and control $I^{(c)}$ inputs. Colors in the raster indicates the group assigned to the synchronous event using an optimal community partition algorithm. c,h) Synchronized Event Transition Matrix, calculated with a window $T_W = 50$ ms and number of events $S_s = 20$. d,i) Projection of the synchronized events in the 2D space spanned by the first two principal components associated to the covariance matrix of the vectors W_s. e,j) Number of coactive cells in each state. The diagonal elements of the bar graph represents the total number of neurons contributing to one state. Panels (a-e) correspond to $g = 8$, while panels (f-j) depict the case $g = 1$. In both cases the system is recorded during the time span required to identify $S_s = 20$. Remaining parameters as in Fig. 1.

In this model v_i is the membrane potential of neuron i, K denotes the number of pre-synaptic connections, $g > 0$ is the strength of the synapses, the variable E_i accounts for the past history of all the previous recurrent post-synaptic potentials (PSP) that arrived to the neuron i at times t_n, and P_i is an auxiliary variable. a_i is the external excitation and α is inversely proportional to the decaying time of the PSP. The inhibition is introduced via the minus sign in front of the synaptic strength in Eq. (2a). The matrix $\mathcal{C}_{i,j}$ is the connectivity matrix where the entry i, j is equal to 1 if there exists a synaptic connection from neuron j to neuron i. When the membrane potential of the q-th neuron arrives to the threshold $v_{th} = 1$, it is reset to the value $v_r = 0$ and the cell emits an α-pulse $p_\alpha(t) = \alpha^2 t \exp(-\alpha t)$ which is instantaneously transmitted to all its post-synaptic neurons. The α-pulses are normalized to one, therefore the area of the transmitted PSPs is conserved by varying the parameter α.

The equations (2a) to (2c) can be exactly integrated from the time $t = t_n$, just after the deliver of the n-th pulse, to time $t = t_{n+1}$ corresponding to the emission of the $(n+1)$-th spike, thus obtaining an *event driven map* [27, 49] which reads as

$$E_i(n+1) = E_i(n)\mathrm{e}^{-\alpha\tau(n)} + P_i(n)\tau(n)\mathrm{e}^{-\alpha\tau(n)} \tag{3a}$$

$$P_i(n+1) = P_i(n)\mathrm{e}^{-\alpha\tau(n)} + \mathcal{C}_{iq}\frac{\alpha^2}{K} \tag{3b}$$

$$v_i(n+1) = v_i(n)\mathrm{e}^{-\tau(n)} + a(1 - \mathrm{e}^{-\tau(n)}) - gH_i(n)\,, \tag{3c}$$

where $\tau(n) = t_{n+1} - t_n$ is the inter-spike interval associated with two successive neuronal firing in the network, which can be determined by solving the transcendental equation

$$\tau(n) = \ln\left[\frac{a - v_q(n)}{a - gH_q(n) - 1}\right]\,, \tag{4}$$

here q identifies the neuron which will fire at time t_{n+1} by reaching the threshold value $v_q(n+1) = 1$.

The explicit expression for $H_i(n)$ appearing in equations (3c) and (4) is

$$H_i(n) = \frac{\mathrm{e}^{-\tau(n)} - \mathrm{e}^{-\alpha\tau(n)}}{\alpha - 1}\left(E_i(n) + \frac{P_i(n)}{\alpha - 1}\right) - \frac{\tau(n)\mathrm{e}^{-\alpha\tau(n)}}{\alpha - 1}P_i(n)\,. \tag{5}$$

The model is now rewritten as a discrete-time map with $3N - 1$ degrees of freedom, since one degree of freedom $v_q(n+1) = 1$, is lost due to the event driven procedure, which corresponds to perform a Poincaré section at any time a neuron fires.

The model so far introduced contains only adimensional units, however, the evolution equation for the membrane potential (2) can be easily re-expressed in terms of dimensional variables as follows

$$\tau_m \dot{V}_i(\tilde{t}) = I_i - V_j(\tilde{t}) - \tau_m G\tilde{E}_i(\tilde{t}) \quad i = 1, \cdots, N \quad ; \tag{6}$$

where we have chosen $\tau_m = 10$ ms as the membrane time constant in agreement with the values reported in literature for MSNs in the up state in mice [50–52], I_i represents the neural excitability and the external stimulations, which takes in account the cortico-thalamic inputs received by the striatal network. Furthermore, $\tilde{t} = t \cdot \tau_m$, the field $\tilde{E}_i = E_i/\tau_m$ has the dimensionality of a frequency and G of a voltage. The currents $\{I_i\}$ have also the dimensionality of a voltage, since they include the membrane resistance.

For the other parameters/variables the transformation to physical units is simply given by

$$V_i = V_r + (V_{th} - V_r)v_i \tag{7}$$

$$I_i = V_r + (V_{th} - V_r)a_i \tag{8}$$

$$G = (V_{th} - V_r)g \tag{9}$$

where $V_r = -60$ mV, $V_{th} = -50$ mV. The isolated i-th LIF neuron is supra-threshold whenever $I_i > V_{th}$, however due to the inhibitory coupling the effective input is $W_i = I_i - \tau_m G\tilde{E}_i$. Therefore, the neuron is able to deliver a spike if $\overline{W}_i > V_{th}$, in this case the firing of the neuron can be considered as mean-driven. However, even if $\overline{W}_i < V_{th}$, the neuron can be lead to fire from fluctuations in the effective input and the firing is in this case fluctuation-driven. It is clear that the fluctuations $\sigma(W_i)$ are directly proportional to the strength of the inhibitory coupling for constant external currents I_i.

For what concerns the PSPs the associated time constant is $\tau_\alpha = \tau_m/\alpha$, and the peak amplitude is given by

$$A_{PSP} = \frac{\alpha}{K}Ge^{-1} = g \times 92 \ \mu V \quad ; \tag{10}$$

where the last equality allows for a direct transformation from adimensional units to dimensional ones, for the connectivity considered in this paper, namely $K = 20$, and for $\alpha = 0.5$, which is the value mainly employed in our analysis. The experimentally measured peak amplitudes of the inhibitory PSPs for spiny projection neurons ranges from $\simeq 0.16 - 0.32$ mV [8] to $\simeq 1 - 2$ mV [28]. These values depend strongly on the measurements conditions, a renormalization of all the reported measurements nearby the firing threshold gives for the PSP peak $\simeq 0.17 - 0.34$ mV [10]. Therefore from Eq. (10) one can see that realistic values for A_{PSP} can be obtained in the range $g \in [2 : 10]$. For $\alpha = 0.5$ one gets $\tau_\alpha = 20$ ms, which is consistent with the PSPs duration and decay values reported in literature for inhibitory transmission among spiny neurons [8, 31]

Our model does not take in account the depolarizing effects of inhibitory PSPs for $V \leq E_{cl}$ [28]. The GABA neurotransmitter has a depolarizing effect in mature projection spiny neurons, however this depolarization does not lead to a direct excitation of the spiny neurons. Therefore our model can be considered as an effective model encompassing only the polarizing effects of the PSPs for $V > E_{cl}$. This is the reason why we have assumed that the membrane potential varies in the range $[-60 : -50]$ mV, since $E_{cl} \simeq -60$ mV and the threshold is $\simeq -50$ mV [28].

In the paper we have always employed dimensional variables (for simplicity we neglect the tilde on the time variable), apart for the amplitude of the synaptic coupling, for which we have found more convenient to use the adimensional quantity g.

Characterization of the firing activity

We define active neurons, as opposite to silent neurons, as cells that deliver a number of spikes larger than a certain threshold $S_\Theta = 3$ during the considered numerical experiments. In particular, we show in Fig. S1 of the Supporting Information that the value of the chosen threshold does not affect the reported results for $0 \leq S_\Theta \leq 100$.

Furthermore, the characterization of the dynamics of the active neurons is performed via the coefficient of variation CV, the local coefficient of variation CV_2 and the zero lag cross-correlation matrix of the firing rates $C(\nu_i, \nu_j)$. The coefficient of variation associated to the i-th neuron is then defined as the ratio:

$$CV^{(i)} = \frac{\sigma(ISI^{(i)})}{\overline{ISI^{(i)}}} \; ;$$

where $\sigma(A)$ and $\overline{A}$ denotes the standard deviation and mean value of the quantity A. The distribution of the coefficient of variation $P(CV)$ reported in the article refer to the values of the CV associated to all the active cells in the network.

Another useful measure of the spike statistics is the local coefficient of variation. For each neuron i and each spike emitted at time $t_n^{(i)}$ from the considered cell the local coefficient of variation is measured as

$$CV_2^{(i)}(n) = \frac{|ISI_n^{(i)} - ISI_{n-1}^{(i)}|}{ISI_n^{(i)} + ISI_{n-1}^{(i)}}$$

where the n-th inter-spike interval is defined as $ISI_n^{(i)} = t_n^{(i)} - t_{n-1}^{(i)}$. The above quantity clearly ranges between zero and one: a zero value corresponds to a perfectly periodic firing, while the value one is attained in the limit $ISI_n^{(i)}/ISI_{n-1}^{(i)} \to 0$ (or $ISI_n^{(i)}/ISI_{n-1}^{(i)} \to \infty$). The probability distribution function $P(CV_2)$ is then computed by employing the values of the $CV_2^{(i)}(n)$ for all the active cells of the network estimated at each firing event, examples of $P(CV_2)$ are shown in Fig. 3(c).

The level of correlated activity between firing rates is measured via the cross-correlation matrix $C(\nu_i, \nu_j)$. The firing rate $\nu_i(t)$ of each neuron i is calculated at regular intervals $\Delta T = 50$ ms by counting the number of spikes emitted in a time window of $10\Delta T = 500$ ms, starting from the considered time t. For each couple of neuron i and j the corresponding element of the $N \times N$ symmetric cross-correlation matrix $C(i, j)$ is simply the Pearson correlation coefficient measured as follows

$$C(i, j) = \frac{cov(\nu_i, \nu_j)}{\sigma(\nu_i)\sigma(\nu_j)} \; ,$$

where $cov(\nu_i, \nu_j)$ is the covariance between signals $\nu_i(t)$ and $\nu_j(t)$, which has been calculated for statistical consistency by employing always spike trains containing 10^7 events. This corresponds to time intervals T_E ranging from 50 s to 350 s (from 90 s to 390 s) for $\Delta V = 5$ mV ($\Delta V = 1$ mV) and $g \in [0.1, 12]$.

State Transition Matrix (STM) and measure of dissimilarity

The STM is constructed by calculating the firing rates $\nu_i(t)$ of the N neurons at regular time intervals $\Delta T = 50$ ms. At each time t the rates are measured by counting the number of spikes emitted in a window $2\Delta T$, starting at the considered time. Notice that the time resolution here used is higher with respect to that employed for the cross-correlation matrix, since we are interested in the response of the network to a stimulus presentation evaluated on a limited time window. The firing rates can be represented as a state vector $R(t) = \{\nu_i(t)\}$ with $i = 1, \ldots, N$. For an experiment of duration T_E, we have $S = \lfloor T_E/\Delta T \rfloor$ state vectors $R(t)$ representing the network evolution ($\lfloor \cdot \rfloor$ denotes the integer part). In order to measure the similarity of two states at different times $t_m = m \times \Delta T$ and $t_n = n \times \Delta T$, we have calculated the normalized scalar product

$$D(m,n) = \frac{R(t_m) \cdot R(t_n)}{|R(t_m)||R(t_n)|} \tag{11}$$

for all possible pairs $m, n = 1, \ldots, S$ during the time experiment T_E. This gives rise to a $S \times S$ matrix called the state transition matrix [53].

In the case of the numerical experiment with two inputs reported in the section *Results*, the obtained STM has a periodic structure of period T_{sw} with high correlated blocks followed by low correlated ones (see Figs. S6(b) and (e) for the complete STM). In Fig 6 (b) is reported a coarse grained version of the entire STM obtained by taking a $4T_{sw} \times 4T_{sw}$ block from the STM, where the time origin corresponds to the onset of one of the two stimuli. The block is then averaged over r subsequent windows of duration $4T_w$, whose origin is shifted each time by $2T_{sw}$. More precisely the averaged STM $\overline{D(m,n)}$ is obtained as follows:

$$\overline{D(m,n)} = \frac{1}{r^2} \sum_{i,j=1}^{r} D(4i+m, 4j+n) \tag{12a}$$

$$\forall\, m, n \leq \lfloor T_{sw}/\Delta T \rfloor \quad .$$

In a similar manner, we can define a dissimilarity metric to distinguish between the response of the network to two different inputs. We define a control input $I^{(c)} = \{I_i^{(c)}\} \in [V_{th},\, V_{th} + \Delta V]$, and we register the network state vectors $R^c(t)$ at S regular time intervals for a time span T_E. We repeat the numerical experiment by considering the same network realization and the same initial conditions, but with a new input $I^{(f)} = \{I_i^{(f)}\}$. The external inputs $I_i^{(f)}$ coincide with the control ones, apart from a fraction f which is randomly taken from the interval $[V_{th},\, V_{th} + \Delta V]$. For the modified input we register another sequence $R^f(t)$ of state vectors on the same time interval, with the same resolution. The instantaneous dissimilarity $d^f(t)$ between the response to the control and perturbed stimuli is defined as:

$$d^f(t_m) = 1 - \frac{R^c(t_m) \cdot R^f(t_m)}{|R^c(t_m)||R^f(t_m)|} \tag{13}$$

its average in time is simply given by $\bar{d}^f = \frac{1}{S}\sum_{i=1}^{S} d^f(t_i)$. We have verified that the average $\bar{d}^f$ is essentially not modified if the instantaneous dissimilarities $d^f(t)$ are evaluated by considering the state vectors $R^c(t_i)$ and $R^f(t_k)$ taken at different times within the interval $[0, t_S]$ and not at the same time as done in (13).

Distinguishability metric Q_d:

Following [17] a metric of the ability of the network to distinguish between two different inputs ΔM_d can be defined in terms of the STM. In particular, let us consider the STM obtained for two inputs $I^{(1)}$ to $I^{(2)}$, each presented for a time lag T_{sw}. In order to define ΔM_d the authors in [17] have considered the correlations of the state vector R taken at a generic time t_{m_0} with all the other configurations, with reference to Eq. (11) this amounts to examine the elements $D(m_0, n)$ of the STM $\forall t_n$. By defining M_1 (M_2) as the average of $D(m_0, n)$ over all the times t_n associated to the presentation of the stimulus $I^{(1)}$ ($I^{(2)}$), a distinguishablity metric between the two inputs can be finally defined as

$$\Delta M_d = |M_1 - M_2| \,. \tag{14}$$

In order to take in account the single neuron variability and the number of active neurons involved in the network dynamics we have modified ΔM_d by multiplying this quantity by the fraction of active neurons and the average

coefficient of variation, as follows

$$Q_d = \Delta M_d \times n^* \times \langle CV \rangle_N \,. \tag{15}$$

The above metric is reported in Figs. 2(c),(d) and Fig. 3 (a).

Synchronized Event Transition Matrix (SETM)

In order to obtain a Synchronized Event Transition Matrix (SETM), we first coarse grain the raster plot of the network. This is done by considering a series of windows of duration $T_W = 50$ ms covering the entire raster plot. A bursting event is identified whenever a neuron i fires 3 or more spikes within the considered window. To signal the burst occurrence a dot is drawn at the beginning of the window. From this coarse grained raster plot we obtain the Network Bursting Rate (NBR) by measuring the fraction of neurons that are bursting within the considered window. When this fraction is larger or equal to the average NBR plus two standard deviations, a synchronized event is identified. Each synchronized event is encoded in the synchronous event vector $W_s(t)$, a N dimensional binary vector where the i-th entry is 1 if the i-th neuron participated in the synchronized event and zero otherwise. To measure the similarity between two synchronous events, we make use of the normalized scalar product between all the pairs of vectors W_s obtained at the different times t_i and t_j in which a synchronized event occurred. This represents the element i, j of the SETM.

Principal Components Analysis (PCA):

In the sub-section *Discriminative and computational capability*, a Principal Component Analysis (PCA) is performed by collecting S state vectors $R(t)$, measured at regular intervals ΔT for a time interval T_E, then by estimating the covariance matrix $cov(\nu_i, \nu_j)$ associated to these state vectors. Similarly, in the sub-section *Physiological relevance for biological networks under different experimental conditions* the PCA is computed by collecting the S_s synchronous event vectors W_s, and the covariance matrix calculated from this set of vectors.

The principal components are the eigenvectors of theses matrices, ordered from the largest to the smallest eigenvalue. Each eigenvalue represents the variance of the original data along the corresponding eigendirection. A reconstruction of the original data set can be obtained by projecting the state vectors along a limited number of principal eigenvectors, obviously by employing the first eigenvectors will allow to have a more faithful reconstruction.

Clustering algorithms.

The *k-means* algorithm is a widespread mining technique in which N data points of dimension M are organized in clusters as follows. As a first step a number k of clusters is defined a-priori, then from a sub-set of the data k samples are chosen randomly. From each sub-set a centroid is defined in the M-dimensional space. at a second step, the remaining data are assigned to the closest centroid according to a distance measure. After the process is completed, a new set of k centroids can be defined by employing the data assigned to each cluster. The procedure is repeated until the position of the centroids converge to their asymptotic value.

An unbiased way to define a partition of the data can be obtained by finding the optimal cluster division [41]. The optimal number of clusters can be found by maximizing the following cost function, termed *modularity*:

$$\mathcal{M} = \frac{1}{A_{tot}} \sum_{ij} \left(A_{ij} - \mathcal{N}_{ij}\right) \delta(c_i, c_j), \tag{16}$$

where, $A \equiv \{A_{i,j}\}$ is the matrix to be clusterized, the normalization factor is $A_{tot} = \sum_{ij} A_{ij}$; $\mathcal{N}_{ij}$ accounts for the matrix element associated to the *null model*; c_i denotes the cluster to which the i-th element of the matrix belongs to, and $\delta(i, j)$ is the Kronecker delta. In other terms, the sum appearing in Eq. (16) is restricted to elements belonging to the same cluster. In our specific study, A is the *similarity matrix* corresponding to the SETM previously introduced. Furthermore, the elements of the matrix $\mathcal{N}$ are given by $\mathcal{N}_{ij} = \eta_i \eta_j / A_{tot}$, where $\eta_i = \sum_j A_{ij}$, these correspond to the expected value of the similarity for two randomly chosen elements [54, 55]. If two elements are similar than expected by chance, this implies that $A_{ij} > \mathcal{N}_{ij}$, and more similar they are larger is their contribution to the modularity $\mathcal{M}$. Hence they are likely to belong to the same cluster. The problem of modularity optimization is NP-hard [56],

nevertheless some heuristic algorithms have been developed for finding local solutions based on greedy algorithms [57–60]. In particular, we make use of the algorithm introduced for connectivity matrices in [54, 61], which can be straightforwardly extended to similarity matrices by considering the similarity between two elements, as the weight of the link between them [62]. The optimal partition technique is used in the sub-section *Physiological relevance for biological networks under different experimental conditions*, where it is applied to the similarity matrix $\mathcal{S}_{ij} = 1 - \mathcal{E}_{ij}$ where the distance matrix $\mathcal{E}_{ij} = \frac{\|x_i^p - x_j^p\|_2}{\max(\mathcal{E})}$. Here x_i^p is the vector defining the i^{th} synchronized event projected in the first p principal components, which accounts for the 80% of the variance.

ACKNOWLEDGMENTS

The authors had useful interactions with Robert Schmidt at an early stage of the project. D.A.-G. and A.T. also acknowledge helpful discussions with Alain Barrat, Yehezkel Ben-Ari, Demian Battaglia, Stephen Coombes, Rosa Cossart, Diego Garlaschelli, Stefano Luccioli, Mel MachMahon, Rossana Mastrandea, Ruben Moreno-Bote, and Viktor Jirsa. This work has been partially supported by the European Commission under the program "Marie Curie Network for Initial Training", through the project N. 289146, "Neural Engineering Transformative Technologies (NETT)" (D.A.-G. and A.T), by the A*MIDEX grant (No. ANR-11-IDEX-0001-02) funded by the French Government "program Investissements d'Avenir" (A.T.), by US National Institutes of Health awards NS078435, MH101697, DA032259 and NS094375 (J.B.), and by "Departamento Adminsitrativo de Ciencia Tecnologia e Innovacion - Colciencias" through the program "Doctorados en el exterior - 2013" (D.A.-G.).

[1] Stephenson-Jones M, Samuelsson E, Ericsson J, Robertson B, Grillner S. Evolutionary conservation of the basal ganglia as a common vertebrate mechanism for action selection. Current Biology. 2011;21(13):1081–1091.
[2] Daw ND, Doya K. The computational neurobiology of learning and reward. Current opinion in neurobiology. 2006;16(2):199–204.
[3] Merchant H, Harrington DL, Meck WH. Neural basis of the perception and estimation of time. Annual review of neuroscience. 2013;36:313–336.
[4] West MJ, Østergaard K, Andreassen OA, Finsen B. Estimation of the number of somatostatin neurons in the striatum: an in situ hybridization study using the optical fractionator method. Journal of Comparative Neurology. 1996;370(1):11–22.
[5] Oorschot DE. Total number of neurons in the neostriatal, pallidal, subthalamic, and substantia nigral nuclei of the rat basal ganglia: a stereological study using the cavalieri and optical disector methods. Journal of Comparative Neurology. 1996;366(4):580–599.
[6] Groves PM. A theory of the functional organization of the neostriatum and the neostriatal control of voluntary movement. Brain Research Reviews. 1983;5(2):109–132.
[7] Beiser DG, Houk JC. Model of cortical-basal ganglionic processing: encoding the serial order of sensory events. Journal of Neurophysiology. 1998;79(6):3168–3188.
[8] Tunstall MJ, Oorschot DE, Kean A, Wickens JR. Inhibitory interactions between spiny projection neurons in the rat striatum. Journal of Neurophysiology. 2002;88(3):1263–1269.
[9] Taverna S, Van Dongen YC, Groenewegen HJ, Pennartz CM. Direct physiological evidence for synaptic connectivity between medium-sized spiny neurons in rat nucleus accumbens in situ. Journal of neurophysiology. 2004;91(3):1111–1121.
[10] Tepper JM, Koós T, Wilson CJ. GABAergic microcircuits in the neostriatum. Trends in neurosciences. 2004;27(11):662–669.
[11] Jaeger D, Kita H, Wilson CJ. Surround inhibition among projection neurons is weak or nonexistent in the rat neostriatum. Journal of neurophysiology. 1994;72(5):2555–2558.
[12] Carrillo-Reid L, Tecuapetla F, Tapia D, Hernández-Cruz A, Galarraga E, Drucker-Colin R, et al. Encoding network states by striatal cell assemblies. Journal of neurophysiology. 2008;99(3):1435–1450.
[13] Carrillo-Reid L, Tecuapetla F, Ibáñez-Sandoval O, Hernández-Cruz A, Galarraga E, Bargas J. Activation of the cholinergic system endows compositional properties to striatal cell assemblies. Journal of neurophysiology. 2009;101(2):737–749.
[14] Guzmán JN, Hernández A, Galarraga E, Tapia D, Laville A, Vergara R, et al. Dopaminergic modulation of axon collaterals interconnecting spiny neurons of the rat striatum. The Journal of neuroscience. 2003;23(26):8931–8940.
[15] Ponzi A, Wickens J. Sequentially switching cell assemblies in random inhibitory networks of spiking neurons in the striatum. The Journal of Neuroscience. 2010;30(17):5894–5911.
[16] Ponzi A, Wickens J. Input dependent cell assembly dynamics in a model of the striatal medium spiny neuron network. Frontiers in systems neuroscience. 2012;6.
[17] Ponzi A, Wickens JR. Optimal balance of the Striatal Medium Spiny Neuron Network. PLoS computational biology. 2013;9(4):e1002954.
[18] Berke JD, Breck JT, Eichenbaum H. Striatal versus hippocampal representations during win-stay maze performance. Journal of neurophysiology. 2009;101(3):1575–1587.

[19] Carrillo-Reid L, Hernández-López S, Tapia D, Galarraga E, Bargas J. Dopaminergic modulation of the striatal microcircuit: receptor-specific configuration of cell assemblies. The Journal of Neuroscience. 2011;31(42):14972–14983.

[20] Izhikevich EM, Moehlis J. Dynamical Systems in Neuroscience: The geometry of excitability and bursting. SIAM review. 2008;50(2):397.

[21] Cummings DM, Cepeda C, Levine MS. Alterations in striatal synaptic transmission are consistent across genetic mouse models of Huntington's disease. ASN neuro. 2010;2(3):AN20100007.

[22] Miller BR, Walker AG, Shah AS, Barton SJ, Rebec GV. Dysregulated information processing by medium spiny neurons in striatum of freely behaving mouse models of Huntington's disease. Journal of neurophysiology. 2008;100(4):2205–2216.

[23] López-Huerta VG, Carrillo-Reid L, Galarraga E, Tapia D, Fiordelisio T, Drucker-Colin R, et al. The balance of striatal feedback transmission is disrupted in a model of parkinsonism. The Journal of Neuroscience. 2013;33(11):4964–4975.

[24] Burkitt AN. A review of the integrate-and-fire neuron model: I. Homogeneous synaptic input. Biological cybernetics. 2006;95(1):1–19.

[25] Burkitt AN. A review of the integrate-and-fire neuron model: II. Inhomogeneous synaptic input and network properties. Biological cybernetics. 2006;95(2):97–112.

[26] Brunel N. Dynamics of Sparsely Connected Networks of Excitatory and Inhibitory Spiking Neurons. J Comput Neurosci. 2000;8(3):183–208.

[27] Zillmer R, Livi R, Politi A, Torcini A. Stability of the splay state in pulse-coupled networks. Phys Rev E. 2007 Oct;76:046102.

[28] Plenz D. When inhibition goes incognito: feedback interaction between spiny projection neurons in striatal function. Trends in neurosciences. 2003;26(8):436–443.

[29] Humphries MD, Wood R, Gurney K. Dopamine-modulated dynamic cell assemblies generated by the GABAergic striatal microcircuit. Neural Networks. 2009;22(8):1174–1188.

[30] Renart A, Moreno-Bote R, Wang XJ, Parga N. Mean-driven and fluctuation-driven persistent activity in recurrent networks. Neural Comput. 2007;19(1):1–46.

[31] Koos T, Tepper JM, Wilson CJ. Comparison of IPSCs evoked by spiny and fast-spiking neurons in the neostriatum. The Journal of neuroscience. 2004;24(36):7916–7922.

[32] Moreno-Bote R, Parga N. Role of synaptic filtering on the firing response of simple model neurons. Physical review letters. 2004;92(2):028102.

[33] Ostojic S. Two types of asynchronous activity in networks of excitatory and inhibitory spiking neurons. Nature neuroscience. 2014;17(4):594–600.

[34] Zillmer R, Livi R, Politi A, Torcini A. Desynchronization in diluted neural networks. Phys Rev E. 2006;74(3):036203.

[35] Jahnke S, Memmesheimer RM, Timme M. How Chaotic is the Balanced State? Front Comp Neurosci. 2009 Nov;3(13).

[36] Monteforte M, Wolf F. Dynamic Flux Tubes Form Reservoirs of Stability in Neuronal Circuits. Phys Rev X. 2012 Nov;2:041007.

[37] Angulo-Garcia D, Torcini A. Stable chaos in fluctuation driven neural circuits. Chaos, Solitons & Fractals. 2014;69(0):233 – 245.

[38] Benettin G, Galgani L, Giorgilli A, Strelcyn JM. Lyapunov characteristic exponents for smooth dynamical systems and for Hamiltonian systems; a method for computing all of them. Part 1: Theory. Meccanica. 1980;15(1):9–20.

[39] Vergara R, Rick C, Hernández-López S, Laville J, Guzman J, Galarraga E, et al. Spontaneous voltage oscillations in striatal projection neurons in a rat corticostriatal slice. The Journal of physiology. 2003;553(1):169–182.

[40] Grillner S, Hellgren J, Menard A, Saitoh K, Wikström MA. Mechanisms for selection of basic motor programs–roles for the striatum and pallidum. Trends in neurosciences. 2005;28(7):364–370.

[41] Newman M. Networks: an introduction. Oxford University Press; 2010.

[42] Jáidar O, Carrillo-Reid L, Hernández A, Drucker-Colín R, Bargas J, Hernández-Cruz A. Dynamics of the Parkinsonian striatal microcircuit: entrainment into a dominant network state. The Journal of Neuroscience. 2010;30(34):11326–11336.

[43] Tecuapetla F, Carrillo-Reid L, Bargas J, Galarraga E. Dopaminergic modulation of short-term synaptic plasticity at striatal inhibitory synapses. Proceedings of the National Academy of Sciences. 2007;104(24):10258–10263.

[44] Laurent G. Olfactory network dynamics and the coding of multidimensional signals. Nature Reviews Neuroscience. 2002;3(11):884–895.

[45] Rabinovich M, Huerta R, Volkovskii A, Abarbanel H, Stopfer M, Laurent G. Dynamical coding of sensory information with competitive networks. Journal of Physiology-Paris. 2000;94(5):465–471.

[46] Rabinovich MI, Varona P. Robust transient dynamics and brain functions. Frontiers in computational neuroscience. 2011;5.

[47] Nowotny T, Rabinovich MI. Dynamical origin of independent spiking and bursting activity in neural microcircuits. Physical review letters. 2007;98(12):128106.

[48] Komarov M, Osipov G, Zhou C. Heteroclinic contours in oscillatory ensembles. Physical Review E. 2013;87(2):022909.

[49] Olmi S, Livi R, Politi A, Torcini A. Collective oscillations in disordered neural networks. Phys Rev E. 2010 Apr;81(4 Pt 2).

[50] Plenz D, Kitai ST. Up and down states in striatal medium spiny neurons simultaneously recorded with spontaneous activity in fast-spiking interneurons studied in cortex–striatum–substantia nigra organotypic cultures. The Journal of Neuroscience. 1998;18(1):266–283.

[51] Klapstein GJ, Fisher RS, Zanjani H, Cepeda C, Jokel ES, Chesselet MF, et al. Electrophysiological and morphological changes in striatal spiny neurons in R6/2 Huntington's disease transgenic mice. Journal of neurophysiology. 2001;86(6):2667–2677.

[52] Planert H, Berger TK, Silberberg G. Membrane properties of striatal direct and indirect pathway neurons in mouse and rat slices and their modulation by dopamine. PloS one. 2013;8(3):e57054.
[53] Schreiber S, Fellous J, Whitmer D, Tiesinga P, Sejnowski TJ. A new correlation-based measure of spike timing reliability. Neurocomputing. 2003;52:925–931.
[54] Newman ME. Fast algorithm for detecting community structure in networks. Physical review E. 2004;69(6):066133.
[55] Humphries MD. Spike-train communities: finding groups of similar spike trains. The Journal of Neuroscience. 2011;31(6):2321–2336.
[56] Fortunato S. Community detection in graphs. Physics Reports. 2010;486(3):75–174.
[57] Ronhovde P, Nussinov Z. Local resolution-limit-free Potts model for community detection. Physical Review E. 2010;81(4):046114.
[58] Reichardt J, Bornholdt S. Statistical mechanics of community detection. Physical Review E. 2006;74(1):016110.
[59] Blondel VD, Guillaume JL, Lambiotte R, Lefebvre E. Fast unfolding of communities in large networks. Journal of Statistical Mechanics: Theory and Experiment. 2008;2008(10):P10008.
[60] Lancichinetti A, Fortunato S. Community detection algorithms: a comparative analysis. Physical review E. 2009;80(5):056117.
[61] Clauset A, Newman ME, Moore C. Finding community structure in very large networks. Physical review E. 2004;70(6):066111.
[62] Newman ME. Analysis of weighted networks. Physical Review E. 2004;70(5):056131.